N 70 21101
NASA CR 108733

SHOCK TUBE SPECTROSCOPY LABORATORY

MEASUREMENTS OF THE VAN DER WAALS Na - λ 5889 IN He WITH A NEWLY DEVELOPED PISTON COMPRESSOR LIGHT SOURCE

NGL-22-007-006

Scientific Report No. 31

CASE FILE COPY

HARVARD COLLEGE OBSERVATORY

60 GARDEN STREET

CAMBRIDGE, MASS

CASE FILE
COPY

MEASUREMENTS OF THE VAN DER WAALS Na - λ 5889 IN He WITH A NEWLY DEVELOPED PISTON COMPRESSOR LIGHT SOURCE

NGL-22-007-006

Scientific Report No. 31

By

Jonathan E. Grindlay

Harvard College Observatory

October 1969

ABSTRACT

A review of the theory of neutral atom broadening in the impact approximation and quasi-static limits is given. The impact approximation is considered in detail and a new calculation for the line width is presented. The result closely resembles that of Griem (1964). A new source of $\sim$ 5000°K helium and (eventually) hydrogen has been developed, using a rapid compression technique. The final (compressed) gas conditions for this piston compressor have been calculated and found to agree approximately with measured values of pressure, temperature, and density. Techniques have also been developed to measure electron densities in this source. The source was used to enable rapid-scanning Fabry-Perot measurements of the half width $\Delta\lambda_p$ of Na - λ 5889 in He over the density range $10^{20} \leqslant N_{He} \leqslant 2.5 \times 10^{20}$ at $\sim$ 4500°K. The measurements showed a linear dependence of $\Delta\lambda_p$ on N_{He}, with the broadening $\sim$ 4.5 greater than the Van der Waals impact approximation prediction. The implications of these results for the astrophysically important case of Fraunhoffer line broadening in hydrogen are discussed.

TABLE OF CONTENTS

I.	INTRODUCTION	1
II.	PRESSURE BROADENING THEORY	10
	A. Van der Waals Interaction	10
	B. Impact Approximation	12
	C. Quasi-Static Approximation	32
III.	EXPERIMENTAL TECHNIQUE	38
	A. Piston Compressor Model	39
	B. Diagnostics	48
	C. Operating Procedure	59
IV.	EXPERIMENTAL RESULTS	64
V.	CONCLUSIONS	72
VI.	ACKNOWLEDGEMENTS	78
	REFERENCES	
	FIGURES	

I. INTRODUCTION

Measurement of the detailed shapes of stellar line profiles provides the most direct technique for ascertaining the physical conditions in the atmosphere of the star in which they are formed. Although in many stars the line profiles cannot be measured accurately, even crude estimates of line widths and displacements give valuable information on the composition and density of the atmosphere. Line profiles may also be used to determine abundances for comparison with values obtained from the curve of growth method. Study of the wings of absorption lines and a subsequent abundance analysis has the advantage that the wings are formed in deeper layers of the photosphere, where atmospheric structure appears better established (Müller, 1967). Probably the most important knowledge to be gained from just line widths alone though is an independent measure of the local density and hence the gravity (Cayrel, 1962), since pressure-broadened line widths must be related to the density of the perturbing gas. This consideration in fact led to the conclusion that the observed broadening of the solar Fraunhoffer lines was due to the radiating (absorbing) atom's collisions with neutral hydrogen atoms,

as the variation in broadening from different atmospheric layers followed the variation in neutral hydrogen density. As indicators of the gravity, measurements of line profiles and an understanding of their form could have even the most general consequences for stellar structure and evolution.

The profiles of absorption lines (or, equivalently, emission lines) are determined primarily by the form of the absorption coefficient, which depends in turn upon the mechanisms for broadening lines. The broadening of spectral lines is a result of all the possible influences on the radiating atom. The effect of its own thermal motion, which broadens the lines statistically, is known as Doppler broadening. Since the broadening $\frac{\Delta\lambda}{\lambda}$ is of order v/c, for thermal velocities ($v \cong 10^5$ cm/sec) of the radiating atom, the Doppler (Gaussian) widths are of order 0.01 Å. Spectral lines are further broadened by radiation damping, which is due to the finite widths of the two energy levels associated with the line. This contribution to the (Lorentzian) width of the line is also of order 0.01 Å. Line broadening also arises from the effects of collisions of either charged or neutral particles with the radiating atom. That in the vast

majority of experimental systems collision broadening is more important than either Doppler broadening or radiation damping is clear from the following argument (Baranger, 1958). In any system in thermal equilibrium in which we observe the absorption or emission of light, the fact that the spectrum is not a blackbody spectrum means that the radiation is not in thermal equilibrium with the system. The thermal equilibrium is then due to interactions through collisions. Because the collisions have to be strong enough to maintain thermal equilibrium in spite of the disruptive effect of the non-equilibrium radiation field, the collisions broaden the line more than the radiation damping.

Theoretical estimates of the broadening due to neutral atoms assume the interaction potential to be Van der Waals of the form $-C_6/R^6$ (Griem, 1964). The magnitude of the ratio of the line width to shift, $\Delta\lambda_{1/2}/d$, serves as a test of this interaction (Van Regemorter, 1965) but it has never been satisfactorily measured for astrophysically significant conditions. Kusch (1958) measured the widths of a few iron lines in hydrogen and found the predicted widths too small by a factor of four, but his source was an iron arc and the question of complete mixing of the Fe and H atoms arises.

Hindmarsh (1959) has measured the value of $\Delta\lambda_{1/2}/d$ for the Ca 4227 Å resonance line in helium and obtains a similar discrepancy with theory, but his measurements were confined to furnace temperatures of ~ 400°K. Finally, Behmenburg (1964) has measured the Na-D (5889 Å) width in He at a helium density of $N_{He} \sim 3 \times 10^{18}$ cm^{-3} and temperature T ~ 2600°K. However his result that the half width was a factor ~ 2 greater than the Van der Waals theory prediction is also somewhat tentative in that his source was a sodium flame immersed in ~ 75% helium and 25% impurity gases (H_2O, CO_2, OH, and CO).

The lack of unambiguous measurements of line widths at various measured perturbing gas densities prompted the present experimental measurements of the broadening of the Na-D (5889 Å) resonance line in helium at T ≃ 4500°K and $N_{He} \simeq 10^{20}$ cm^{-3}. The sodium resonance line was chosen because of its strength in stellar spectra and the ease with which its profile may be measured to yield neutral hydrogen densities and hence stellar gravities. The broadening was measured in He rather than H because a monatomic gas is heated more efficiently than a diatomic gas by an adiabatic compression, which was the technique used to achieve high temperatures while maintaining low

electron densities and hence negligible Stark broadening. The present design of this new piston compressor (as discussed in Section III) light source enables us to measure broadening in He at 5000°K with $N_{He} \geq 10^{20}$ cm^{-3}, and while it was possible to measure line half-widths simultaneously with T and N_{He}, it was not possible to measure the shift, d. An improved piston compressor now under construction should permit half-width (and possible shift) measurements of the Na-D and other astrophysically interesting (e.g. Mg-B) lines in H at $N_H \sim 10^{20}$ cm^{-3} and in He at $N_{He} \sim 5 \times 10^{18}$ cm^{-3}.

Many authors have contributed to the general theory of pressure broadening by neutral atom collisions. The first treatment of line broadening was, of course, that of Lorentz in 1906, and is known as the impact theory of collision broadening. This treatment, as did those subsequently of Weisskopf (1932) and Lindholm (1941), essentially regards a collision as giving rise to an "abrupt" phase change (of infinity (Lorentz) or of unity (Weisskopf)) in the radiation emitted. The phase shift criteria for such collisions, which occur at a frequency ν and are statistically independent, are then formulated in terms of a "collision diameter" ρ, which involves the

interaction potential between the perturber and initial state of the radiating electron. The line width by this Lorentzian theory is then just ν, since we may view the line width as being the inverse of the time required for the light to lose "memory" of its original phase. Thus in this Lorentzian limit of complete interruptions of the wave train, no shift of the line center is predicted. However, a more general study of this fast collisional approximation or "impact approximation", which we shall review in Section II, does predict a shift.

At the other extreme from the calculations of line profiles using the impact approximation are those using the "quasi-static approximation", introduced by Holtsmark (1919) and developed subsequently by many others. These calculations proceed by first assuming all the perturbers are at fixed positions shifting the spectrum of sharp lines. Then one performs a statistical average over positions, which gives a broadened spectrum. Such a procedure is clearly admissible if phase changes are large in times short compared to a "collision time", defined as b/v where v is the perturber's velocity and b the impact parameter. The important difference in these two theories is in their prediction of the variation of half-width with perturber density: the impact approximation results are linear in

N, while the quasi-static results are approximately quadratic (Margenau, 1935).

The difference between the ranges of validity of these two limiting approximations may be expressed in terms of the relationship between collision frequency and collision time. The Lorentz impact theory requires statistically independent "strong" collisions that produce large phase shifts. To be independent, they must be well-separated in time in comparison with the collision time. Thus the impact approximation is generally valid if strong collisions occur at intervals much longer than the collision time, whereas the quasi-static approximation is good if strong collisions occur frequently. The implications are then that the quasi-static approximation will be valid at high perturber densities and far in the wings of the line. The validity of the impact approximation requires a typical collision (not contributing to the broadening) to be "weak", i.e., the product of the interaction potential by the collision time must be less than $\hbar$. This insures that the collision can be treated by perturbation theory and does not produce much of a disturbance (Baranger, 1962), and that the occasional strong collisions causing the broadening are statistically independent.

Before discussing line broadening calculations, we estimate which of these two approximations is most likely to apply to the experimental conditions expected for our measurements of pressure-broadened line widths. Our discussion shows that there will be a limitation on how far out in the wings of a broadened line the impact approximation will apply, since the validity condition requires the level lifetime ($\sim \frac{1}{\Delta\omega}$) to be much greater than the collision time, i.e.

$$\Delta\omega = \omega - \omega_o << \tau^{-1} \tag{1}$$

where ω_o is the frequency at line center, ω the frequency in the wing, and τ the collision time. However, the finite size of wave packets (Baranger, 1962), which are necessarily large compared to λ, gives the condition

$$\tau >> \hbar/\epsilon \simeq \hbar/kT \tag{2}$$

If we combine (1) and (2) and solve for $\Delta\lambda$, we obtain for the wave length interval out in the wing,

$$\Delta\lambda = \frac{\lambda^2 \Delta\omega}{2\pi c} << \frac{\lambda^2 kT}{2\pi\hbar c} \tag{3}$$

This may be evaluated for the Na-D_2 line at 5889 Å in a gas at 5000°K to give a very approximate upper limit on the validity of the impact approximation of $\Delta\lambda << 1000$ Å The actual calculation for the line width we shall describe, using the impact approximation, imposes more definite limits. Our experimental conditions are somewhat borderline for the impact approximation and we present also a brief treatment of the quasi-static approximation calculation for the line width.

II. PRESSURE BROADENING THEORY

A. Van der Waals Interaction

An undisturbed atom radiating at frequency $\nu_0 = (E_1 - E_2)/h$ will radiate at $\nu' = [E_1(R) - E_2(R)]/h$ when the energy levels E_1 and E_2 are perturbed by an atom at R. Since $E_1 - E_2$ changes with R, $\nu' \neq \nu_0$ and the spectral line is shifted. Since throughout a radiating volume emission will occur at different R values, the line is broadened also.

We may specify the interaction responsible for these energy level shifts as a function of R only. The interaction between neutral atoms A and B at large separations may be described as a series of interactions between the various instantaneous multipole moments. If atom B has no multipole moment, as is the case for He or H in their ground states, the interaction potential may simply be taken to be Van der Waals and of the form

$$V(R) \sim \frac{C_6}{R^6} \tag{4}$$

This follows from the standard multipole expansion of V(R) retaining only the long range term describing the second order dipole-dipole interaction.

The interaction constant C_6 is derived (e.g. see Margenau and Kestner, 1969) from second order perturbation theory. The condition for the validity of this derivation may be expressed as:

$$\Delta E_B >> \Delta E_A \tag{5}$$

where ΔE_B is the excitation energy of the perturber B and ΔE_A that of the radiation A. This condition is satisfied for the Na-D transition in He and H. The constant C_6, as we shall later show (Eq. (50)), is then given by

$$C_6 = e^2 \alpha_B < r_A^2 > \tag{6}$$

where α_B is the dipole polarizability of B and $< r_A^2 >$ is the average value of r^2 for the states of A undergoing the interaction.

To this attractive Van der Waals potential, a short-range repulsive core may be added to give the Lennard-Jones potential

$$V(R) = - \frac{C_6}{R^6} + \frac{C_{12}}{R^{12}} \quad . \tag{7}$$

The R^{-12} dependence of the repulsive part is chosen for analytical convenience. The constant C_{12} may be given in terms of C_6 and a specified depth D (in ev.) of the potential

$$C_{12} = \frac{6.801}{D} C_6^2 \tag{8}$$

so that here the units of C_6 are ev - cm^6 and those of C_{12} are ev - cm^{12}.

B. Impact Approximation

The calculation of the line shape given here is based on the work of Baranger (1958a).

In accordance with the discussion of the impact approximation given above, we assume that the radiating atom is fixed with the perturbers moving around it. The wave function for the whole system is taken to be the product of the internal wave function of the atom and of a function of the center of mass coordinates (R_1 --- R_n) of the perturbers:

$$\Psi = U(R_A)\psi(R_1 \ldots R_n) \ . \tag{9}$$

This is the Born-Oppenheimer approximation and it is valid for this problem as the perturbers are atoms and thus much heavier than the electrons of the atom.

The interaction potential $V(R_1 \text{ --- } R_n)$ determines the motion of the perturbers near the atom. We assume that the perturbers interact only with the atom and are statistically independent of each other. This is again reasonable for neutral atoms at low densities. Further, the calculation requires "scalar additivity" of the potentials,

$$V(R_1 \cdots R_n) = V(R_1) + \cdots + V(R_n), \tag{10}$$

in accordance with the tenet of the impact approximation that only one perturber at a time undergoes "strong collisions" with the radiator A. Since the scalar additivity criterion is satisfied for long range Van der Waals forces (Baranger, 1958a), the interaction potential used here, Eq. (4), satisfies Eq. (10).

With the foregoing assumptions it is then reasonable to consider (Weisskopf, 1932, Jablonski, 1945) the whole system as a single quantum mechanical object with certain energy levels and stationary states. The power radiated

by dipole transitions from state i to f of each of the radiators is given by

$$P_A(\omega) = \frac{4\omega_{if}^4}{3c^3} \; |< f|d|i >|^2 \qquad (11)$$

where $\omega_{if} = E_i - E_f$ is the frequency and d the radiator's dipole moment. The spectrum of the whole system is obtained by summing over all possible final states f and averaging over initial states i, which are distributed with probabilities ρ_i, say. Thus the power per unit frequency interval, $P(\omega)$ is

$$P(\omega) = \frac{4\omega^4}{3c^3} \; F(\omega) \qquad (12)$$

where

$$F(\omega) = \sum_{if} \delta(\omega - \omega_{if}) |< f|d|i >|^2 (\rho_{i_1} \cdots \rho_{in}) \qquad (13)$$

and the probabilities ρ_i are given by a constant times the Boltzmann factor $e^{-Ei/kT}$.

The initial (i) and final (f) wave functions have the form (9). The additivity assumption of (10) means that we may decompose the perturber wave functions

$$\psi(R_1 \cdots R_n) = \psi(R_1)\psi(R_2) \cdots \psi(R_n) \tag{14}$$

where each factor is a solution of a Schrödinger equation with potential V_i. For each perturber, though, there are two potentials -- one for each state of the radiating atom. Therefore

$$(K_1 + V_i)\psi_{i1}(R_1) = \epsilon_1 \psi_{i1}(R_1) \tag{15}$$

$$(K_1 + V_f)\psi_{f1}(R_1) = \epsilon_1' \psi_{f1}(R_1)$$

are the Schrodinger equations for perturber 1, say, with , its total kinetic energy and ϵ_1 the total energy. The initial wave function for the whole system, Eqs. (9) and (14), is then

$$U_i(R_A)\psi_{i1}(R_1)\psi_{i2}(R_2) \cdots \psi_{in}(R_n) \tag{16a}$$

with energy

$$E_i + \epsilon_1 + \epsilon_2 + \cdots + \epsilon_n \tag{16b}$$

and the final wave function is

$$U_f(R_A)\psi_{f_1}(R_1)\psi_{f_2}(R_2)\cdots\psi_{fn}(R_n) \tag{17a}$$

with energy

$$E_f + \epsilon_1' + \epsilon_2' + \cdots \epsilon_n' \tag{17b}$$

We substitute expressions (16) and (17) into (12) and (13) to obtain the power spectrum

$$P(\omega) = \sum_{if}\left(\frac{4\omega^4}{3c^3}\right) |< U_f|d|U_i >|^2 \cdot |< \psi_{f_1}|\psi_{i_1} >|^2 \cdot\cdot$$

$$\cdot\cdot\ |< \psi_{fn}|\psi_{in} >|^2 (\rho_{i_1}\cdots\rho_{in}) \tag{18}$$

and the frequency emitted is

$$\omega_{if} = E_f - E_i + (\epsilon_1' - \epsilon_1) + \cdots + (\epsilon_n' - \epsilon_n) \tag{19}$$

Thus the frequency is shifted from its unperturbed value of $(E_f - E_i)$ because energy may be used for increasing or decreasing the total kinetic energy of the perturbers.

In order to isolate effectively these frequency shifts it is desirable to include explicitly these frequency (energy) components in our formulation. This is easily accomplished by taking the Fourier transform of (13).

$$\Phi(s) = \int_{-\infty}^{\infty} F(\omega) e^{-i\omega s} d\omega$$

$$= \sum_{if} \int_{-\infty}^{\infty} \delta(\omega - \omega_{if}) |< f|d|i >|^2 (\rho_{i1} \cdots \rho_{in}) e^{-i\omega s} d\omega$$

$$= \sum_{if} |< f|d|i >|^2 (\rho_{i1} \cdots \rho_{in}) e^{-i\omega_{if} s} \quad . \tag{20}$$

If we substitute in the factorization that gave Eq. (18) and use (19) with the origin of frequency redefined at line center (i.e. dropping $E_i - E_f$), we obtain to within a constant factor, $|< U_f|d|U_i >|^2$,

$$\Phi(S) = \sum_{if} (\rho_{i1} \cdots \rho_{in}) |<\psi_{f1}|\psi_{i1}>| \cdots |<\psi_{fn}|\psi_{in}>|^2$$

$$\times \exp\left[-i[(\epsilon_1' - \epsilon_1) + \ldots + (\epsilon_n' - \epsilon_n)]\right] \tag{21}$$

Thus $\Phi(s)$ turns out to be the nth power of another function $\varphi(s)$, which refers to a single perturber

$$\Phi(s) = [\varphi(s)]^n$$

$$\varphi(s) = \sum_{if} \rho_i |< \psi_f | \psi_i >|^2 e^{-i(\epsilon'-\epsilon)s} \quad . \tag{22}$$

This result is a direct consequence of our assumption of scalar additivity of the interaction potentials or the statistical independence of the perturbing collisions.

As $\Phi(s)$ is the Fourier transform of the line shape or power spectrum, $F(W)$, by the Wiener-Khintchine Theorem $\Phi(s)$ is just the autocorrelation function of the light amplitude, $A(t)$. To see this (Baranger, 1962), write the light train as a sum of monochromatic waves

$$A(t) = \int_{-\infty}^{\infty} e^{-i\omega t} a(\omega) d\omega \quad .$$

Then the autocorrelation function is the statistical average

$$C(t) = [A(t+s)A^*(t)]_{av} = \iint d\omega d\omega' e^{i(\omega' t - \omega(t+s))} [a(\omega)a^*(\omega')]_{av} \quad .$$

Since there is no phase relation between frequencies $\omega \neq \omega'$,

$$[a(\omega)a^*(\omega')]_{av} = P(\omega) \simeq \delta(\omega-\omega')F(\omega)$$

where we have again neglected the slowly varying factor ($\omega \approx$ const.) $4\omega^4/3C^3$. Substituting this into the equation for C(t) and using (20) we obtain

$$C(t) = \Phi(s) \tag{23}$$

Returning now to the calculation of $\varphi(s)$, we reason that a single perturber will be in the vicinity of a particular radiating atom for a fraction of the time inversely proportional to the gas volume V. Since without perturbation, the line shape $F(\omega)$ corresponds to $\varphi(s) = 1$, we may then generally write

$$\varphi(s) = 1 - V^{-1}g(s) \tag{24}$$

where g(s) is a function whose form (Eq. (31)) we now derive. From Eq. (22) and the expression for the density N of the perturbers $N = n\ V^{-1}$,

$$\Phi(s) = \exp[-Ng(s)] \quad . \tag{25}$$

Thus by expressing $\varphi(s)$ in the form of (24), the line shape follows from a Fourier transform of (25). Introducing the Hamiltonians for a perturber when the radiating atom is in its initial state

$$H_i = K + V_i \tag{26a}$$

and the perturber's Hamiltonian for the radiator in its final state

$$H_f = K + V_f \tag{26b}$$

we can eliminate the explicit dependence on the final states f from Eq. (22) for $\varphi(s)$:

$$\begin{aligned}\varphi(s) &= \sum_{if} \rho_i \, \langle \psi_i | \psi_f \rangle e^{i\epsilon' s} \langle \psi_f | \psi_i \rangle e^{-i\epsilon s} \\ &= \sum_i \rho_i \langle \psi_i | e^{iH_f s} \, e^{-iH_i s} | \psi_i \rangle\end{aligned} \tag{27}$$

Furthermore, the average over the initial states indicated by $\psi\rho_i$ may be postponed until the end of the calculation for the line width when an appropriate average with the Boltzmann factor should be taken. Also the wave functions

ψ_i are normalized now to the volume of the gas V instead of unity as in (27). These two steps give

$$\varphi(s) = V^{-1}\langle\psi_i|e^{iH_f s}e^{-iH_i s}|\psi_i\rangle \tag{28}$$

Then using the integral equation identity (Baranger, 1958)

$$e^{iH_f s}e^{-iH_i s} = 1 - i\int_0^s dt\, e^{iH_f t}\Delta V e^{-iH_i t} \tag{29}$$

where

$$\Delta V = V_i - V_f = H_i - H_f \tag{30}$$

and substituting into Eq. (28), one obtains

$$\varphi(s) = 1 - i\,V^{-1}\int_0^s dt e^{-i\epsilon t}\langle\psi_i|e^{iH_f t}\Delta V|\psi_i\rangle \tag{31}$$

where $e^{-iH_i t}$ has been taken out of the matrix element. Comparing Eq. (31) with Eq. (24), we may write g(s):

$$g(s) = i\int_0^s dt e^{-i\epsilon t}\langle\psi_i|e^{iH_f t}\Delta V|\psi_i\rangle \tag{32}$$

At this point we make the further approximation that there is negligible perturber interaction with the lower

state of the radiative transition and thus $V_f \cong 0$. It is not essential to make this assumption and Baranger (1958) carries the derivation through for perturbation of both states, but the approximation leads to analytical expressions for the width and shift that are considerably easier to evaluate. The approximation is generally a good one since the radiating atom is more tightly bound and less polarizable in the lower state than in the upper one. Thus according to (26b), H_f in (32) may now be replaced by K. Also, for large enough t, $\langle\psi_i|e^{iKt} \rightarrow \langle\psi_i|e^{i\epsilon t}$ and as this is just the basic assumption of the impact approximation, i.e. that $t >> \tau$, we may write

$$g(s) \simeq i \int_0^s dt \, \langle\psi|V|\psi\rangle, \quad s >> \tau \tag{33}$$

where we have dropped the subscript i from ψ and V.

We now have the choice of either further approximating (33) by assuming the matrix element is roughly constant (Baranger, 1958a), or attempting to evaluate the integral letting $s \rightarrow \infty$. Both approaches will be discussed.

An immediate expression for the line shape $F(\omega)$ comes from considering the matrix element of (33) to be roughly constant. Then

$$g(s) \simeq is \langle\psi|V|\psi\rangle = is \langle k|V|\psi\rangle \tag{34}$$

where we have written the upper state wave function as a plane wave k near the origin (i.e. for large t). Then Eq. (25) gives the autocorrelation function

$$\Phi(s) = \exp[-iN \langle k|V|\psi\rangle s] \tag{35}$$

This has as its Fourier transform the Lorentzian line shape,

$$F(\omega) = \frac{1}{\pi} \frac{\Delta\omega_{\frac{1}{2}-\frac{1}{2}}}{(\omega-d)^2 + (\Delta\omega_{\frac{1}{2}-\frac{1}{2}})^2} \tag{36}$$

with the (half-half) width $\Delta\omega_{\frac{1}{2}-\frac{1}{2}}$ given by

$$\Delta\omega_{\frac{1}{2}-\frac{1}{2}} = -N \text{ Im } \langle k|V|\psi\rangle \tag{37}$$

and the shift d

$$d = N \text{ Re } \langle k|V|\psi\rangle \tag{38}$$

Now the matrix element $\langle k|V|\psi\rangle$ is proportional to the forward scattering amplitude

$$f(\theta, \phi) = - \frac{m}{2\pi} < k' | V | \psi > \tag{39}$$

where k' makes the angles θ and ϕ with k and has the same magnitude as k. Thus (37) and (38) become

$$d = - \frac{2\pi N}{m} \mathrm{Re}[f(0)]_{Av} \tag{40}$$

$$\Delta\omega_{\frac{1}{2}-\frac{1}{2}} = \frac{2\pi N}{m} \mathrm{Im}[f(0)]_{Av} \tag{41}$$

where "Av" designates the Boltzmann average over initial states that was postponed earlier.

Finally, the broadened line width may be written in terms of σ, the total cross section, by making use of the optical theorem

$$\mathrm{Im}[f(0)] = \frac{k}{4\pi} \int d\Omega |f(\Omega)|^2 = \frac{k}{4\pi} \sigma \quad . \tag{42}$$

Since $v = k/m$, the width is

$$\Delta\omega_{\frac{1}{2}-\frac{1}{2}} = (\tfrac{1}{2} Nv\sigma)_{Av} \quad . \tag{43a}$$

The quantum mechanical cross section σ may be written as twice the classical cross section $\pi\rho_{min}^2$, allowing for diffraction effects, giving

$$\Delta\omega_{\frac{1}{2}-\frac{1}{2}} = (\pi\rho_{min}^2 \bar{v} N) \tag{43b}$$

Physically ρ_{min} corresponds to the limiting impact parameter dividing the regimes of weak and strong collisions, for which the impact approximation is valid. As Eq. (43b) is just the expression for the collision frequency, the width obtained here is just that of the Lorentz theory discussed above. However, the following new calculation for ρ_{min} will give a different result than the Lorentz theory, although similar to that obtained by Griem (1964).

We begin again with Eq. (33) above. Letting s go to infinity, i.e. in the limit of the impact approximation $s >> \tau$, we obtain the approximate equation

$$g(\infty) = 1 \simeq \int_{-\infty}^{\infty} dt |< \alpha | V_{eff} | \alpha >| \tag{44}$$

The wave functions α of Eq. (44) then refer to the entire system, i.e. to states a of the radiating atom and states b of the perturber.

Eq. (44) was derived from Eq. (23) and the mathematical fact that (Bracewell, 1965)

$$\lim_{t\to\infty} C(t) = \lim_{s\to\infty} \Phi(s) = \lim_{s\to\infty} \int_{-\infty}^{\infty} e^{i\omega s} F(\omega)\, d\omega = 0 \qquad (45)$$

which means physically just that the duration of light emission is finite, a necessary condition for $F(\omega)$ to be square integrable. Then, from Eq. (22)

$$\lim_{s\to\infty} \varphi(s) = 0$$

and thus by Eq. (24)

$$\lim_{s\to\infty} g(s) = \lim_{s\to\infty}[V - V\,\varphi(s)] = V = i \int_0^{\infty} dt \langle \psi | V | \psi \rangle \quad .$$

Eq. (44) follows then from again normalizing the wave functions to the volume of the system V and taking the absolute value.

We continue now by substituting into Eq. (44) the second order perturbation theory expansion of the interaction matrix element

$$1 = \int_{-\infty}^{\infty} \frac{dt}{\hbar} \sum_{a'b'} \frac{\langle a,0|V|a'b'\rangle \langle a'b'|V|a,0\rangle}{\Delta E_b} \qquad (46)$$

where we have now changed from atomic units back to cgs with the introduction of $\hbar$ (since until now $E = \omega$). However, as was indicated in writing Eqs. (4) and (5), we may expand (46) by neglecting the energy splitting of A and factoring the matrix element

$$\sum_{a'b'} \frac{< a,0|V|a',b' > < a',b'|V|a,0 >}{\Delta E_b} \tag{47}$$

$$= \frac{e^2}{R^6} \sum_{a'} < a|v_1^A|a' > <a'|v_1^A|a > \sum_{b'} \frac{< 0|v_1^B|b' > < b'|v_1^B|0 >}{E_{b'} - E_o}$$

where the (one electron) dipole-dipole interaction energy is given in terms of the dipole operator v_1 by (Dalgarno, 1967)

$$v_1^A = e\eta_a \, Y_{1\mu}(r_a)$$

$$V = V_{\substack{\text{dipole-}\\\text{dipole}}} = \frac{4\pi}{3} \sum_{\mu} \frac{2!\, v_1^A v_1^B}{(1-\mu)!\,(1+\mu)!} \tag{48}$$

$$v_1^B = e\eta_b \, Y_{1-\mu}(r_b)$$

Here μ is the magnetic quantum number and r_a and r_b refer to the radii of the states of the radiator A and

perturber B. Thus (47) may be written in terms of the dipole polarizability of the perturber B

$$\alpha_B = \frac{2}{3} e^2 \sum_{b'} \frac{| < 0|r_b|b' > |^2}{E_{b'} - E_o} \tag{49}$$

and the square of the matrix element of the coordinate vector of the (upper) perturbed level of A

$$< r_A^2 > = < a|r_a \cdot r_a|a > = \quad < a|r_a|a' > < a'|r_a|a >$$

giving the Van der Waals interaction of Eqs. (4) and (6),

$$< \alpha|V_{eff}|\alpha > = \frac{e^2 \alpha_B < r_A^2 >}{R^6} = \frac{C_6}{R^6} \tag{50}$$

where we have summed over the magnetic quantum number μ. Substituting (50) into (44) yields then

$$1 = \frac{e^2 \alpha_B < r_A^2 >}{\hbar} \int_{-\infty}^{\infty} \frac{dt}{R^6} \quad . \tag{51}$$

To do the integral over the interatomic distance R, we may treat the perturbers as classical particles that do not perturb the emitter except during the very short collision time. Thus in terms of the impact parameter

ρ_{min} for these collisions

$$R(t) = [\rho_{min}^2 + \bar{v}^2 t^2]^{\frac{1}{2}} \tag{52}$$

where the mean relative velocity is

$$v = \left[\frac{8kT}{\pi M} \left(\frac{1}{A_A} + \frac{1}{A_B} \right) \right]^{\frac{1}{2}} . \tag{53}$$

Here M is the nuclear mass, T is the temperature, and A_A and A_B are the atomic weights of A and B. Using (52) in the integral of (51) we then obtain

$$1 = \frac{3\pi \ e^2 \alpha_B \ < r_A^2 >}{8 \ \hbar \ \bar{v} \ \rho_{min}^5}$$

or,

$$\rho_{min} = \left[\frac{3\pi \ e^2 \alpha_B \ < r_A^2 >}{8 \ \hbar \ \bar{v}} \right]^{1/5} . \tag{54}$$

Thus Eq. (43b) for the half-half width in angular frequency units of the Van der Waals broadened line arising from the perturbed upper level of atom A is

$$\Delta\omega_{\frac{1}{2}-\frac{1}{2}} = \pi\rho_{min}^2 \bar{v} N = \pi N \left[\frac{3\pi C_6}{8\hbar}\right]^{2/5} \bar{v}^{3/5} \tag{55}$$

or

$$\Delta\omega_{\frac{1}{2}-\frac{1}{2}} = \pi N \left[\frac{3\pi e^2 \alpha_B < r_A^2 >}{8\hbar}\right]^{2/5} \bar{v}^{3/5} . \tag{55a}$$

This result is very nearly that obtained by Griem (1964). To see this, we note that in terms of the oscillator strength

$$f_{ob'} = \frac{2}{3} (E_{b'} - E_i) \frac{m}{\hbar^2} |< 0|r_b|b' >|^2 \tag{56}$$

for transitions from the ground state (0) to excited states (b') of the perturber B, Eq. (49) for the polarizability becomes

$$\alpha_B = \frac{\hbar^2 e^2}{m} \sum_{b'} \frac{f_{ob'}}{(E_b - E_o)^2} \simeq \frac{\hbar^2 e^2}{m E_{b'}^2} . \tag{57}$$

where m is the electron mass.

Here we have approximated the sum of $f_{ob'}$ over the possible excitations of B by unity. Further, we note that the one-electron approximation allows us to rewrite the $< r_A^2 >$ term in (50) (Bethe and Salpeter, 1955).

$$< r_A^2 > = a_o^2 \bar{R}_A^2 \simeq \frac{a_o^2}{2} \cdot \frac{E_H}{E_\infty - E_a} \left[\frac{5E_H}{E_\infty - E_a} + 1 - 3\ell_a(\ell_a + 1) \right] \tag{58}$$

where $a_o = h^2/me^2$, E_H and E_∞ are the ionization potentials of the hydrogen and the radiator A, respectively and where E_∞ is the excitation energy of the perturbed (upper) level of A and ℓ_a its orbital quantum number.

Substituting (57) and (58) into Eq. (55a) one obtains

$$\Delta\omega_{\frac{1}{2}-\frac{1}{2}} = \pi N \left[\frac{3\pi \hbar^5 R_A^2}{8m^3 E_b^2} \right]^{2/5} \bar{v}^{3/5} \tag{59}$$

which differs from Griem's (1964) result only by a factor $3/2^{2/5} \cong 1.18$. Both our result and Griem's are limited to the range of validity of the impact approximation from which we started. Although the results are admittedly only approximate in that the broadening of the lower state is neglected and the interaction contains no short range repulsive part (e.g. Eq. (7)), we suggest that the result obtained here in the form given in Eq. (55) might be more useful in that the approximation of (57) is not required and the polarizabilities α_B are known accurately for the perturbers of interest, hydrogen and helium. We note that the impact approximation requirements that the collision

time be much less than the time between collisions gives the condition on N for the validity of (55) or (59)

$$N << \frac{1}{\pi}\left[\frac{8m^3\ \bar{v}\ E_{b'}^2}{3\pi\hbar^5\ \bar{R}_A^2}\right]^{3/5} . \qquad (60)$$

For densities approaching or exceeding this limit, we must turn to the quasi-static approximation to estimate the neutral atom pressure broadening.

C. Quasi-Static Approximation

At higher perturber densities multiple interactions become important and the line widths are no longer linearly dependent on density. The standard approach (Holtsmark, 1919) for calculating the perturbation of a radiating atom in the high density region is to consider the radiator and perturbers at rest, and the frequency emitted by the radiating atom A at each position r is simply given by $(V_a(r) - V_{a'}(r))/\hbar$, $V_a(r)$ and $V_{a'}(r)$ being the potential energies of A in the initial and final states, respectively. The potential energy $V_a(r)$ of the radiating atom is taken to be the sum of the unperturbed energy E_o, say, and the perturbation energies due to all the perturbers. These

perturbation energies are again assumed to be additive, and a function of the perturber positions R_i.

$$V_a(r) = E_o + \sum_i \frac{C_6}{R_i^6} U(\xi_i) \quad . \tag{61}$$

Here we have once again taken the interaction to be Van der Waals; $U(\xi_i)$ is a function with vanishing mean denoting the dependence on angle and spin (Margenau, 1951). The frequency difference $\Delta\omega$ from the natural frequency is then

$$\Delta\omega = \sum_i \frac{C_6}{\hbar R^6} U(\xi_i) \tag{62}$$

where C_6 refers now only to the excited state since we again neglect the broadening of the ground state. The variation of intensity with $\Delta\omega$ is determined by the probability $I(\Delta\omega)$ that in the presence of n perturbers the potential energy

$$\sum_i \frac{C_6}{R^6} U(\xi_i)$$

shall have the value $\hbar\Delta\omega$. We may assume (Ch'en and Takeo, 1957) this probability is proportional to the time interval

during which $\Delta\omega$ is radiated. Now since the perturbers are considered at rest, the radiation field may be expressed as a plane wave average

$$A_n(t) = \exp\left[i \sum_{i=1}^{n} \frac{C_6}{R^6} U(\xi_i) \right] \tag{63}$$

$$= \left\{ \int_{-1}^{+1} \rho(\xi) d\xi \int_{0}^{R} \rho(R) dR \exp\left[\frac{iC_6}{R^6} U(\xi) \right] \right\}^n$$

where the probability densities with respect to R_i and ξ_i are given by (Margenau, 1951)

$$\rho(R_i)dR_i = \frac{3R_i^2 \, dR_i}{R_o^2} , \quad \rho(\xi_i)d\xi_i = \frac{1}{2} d\xi_i$$

if the gas volume is $4/3 \, \pi \, R_o^3$ and $U(\xi_i) = \pm 1$. Then the Fourier transform with respect to t gives the probability distribution $I(\Delta\omega)$ or line shape

$$I(\Delta\omega) = \frac{1}{2\pi} \int_{-\infty}^{\infty} e^{-i\Delta\omega t} A_n(t) dt .$$

Margenau (1935) evaluated this expression and found that

$$I(\Delta\omega) = \frac{1}{\pi} \int_0^\infty \exp(-Ng_6 t^{\frac{1}{2}}) \cos \Delta\omega t \, dt \qquad (64)$$

where N is the perturber density and where

$$g_6 = \frac{2\pi}{3} \left[\frac{2\pi C_6}{\hbar}\right]^{\frac{1}{2}} .$$

The intensity distribution is symmetric about the line center ($\Delta\omega = 0$) with central intensity

$$I(0) = \frac{2\pi}{(Ng_6)^2}$$

which suggests that the half-width increases roughly with N^2. In fact, Margenau's calculations show that the broadening due to multiple interactions between spherical, non-polar atoms gives a half-width varying as

$$\Delta\omega_{\frac{1}{2}} = .822 \, \pi^3 \left|\frac{C_6}{\hbar}\right| N^2 \quad . \qquad (65)$$

Upon substituting in Eq. (50) for C_6, we obtain

$$\Delta\omega_{\frac{1}{2}} = .822\pi^3 \left|\frac{e^2 \alpha_B < r_A^2 >}{\hbar}\right| N^2 \qquad (65a)$$

It is interesting to compare this estimate with that obtained for lower densities by the impact approximation. The ratio of this quasi-static estimate for the line width to the impact approximation result of Eq. (55) is then

$$\frac{\Delta\omega_{static}}{\Delta\omega_{impact}} \simeq 10^{-22} N \qquad (66)$$

where we have evaluated the expression for a typical astrophysically interesting temperature of 5000°K for which $\bar{v}^{-3/5} \cong 10^3$. This suggests that the impact approximation for neutral atom broadening might be useful up to perturber densities $N \leqslant 10^{22}$ cm^{-3}. The upper limit on N given by (60) predicts similar limits for the impact approximation.

Before concluding this somewhat lengthy discussion of pressure broadening theory, we call attention to the fact that regardless of density-limiting approximation to be used, the Van der Waals interaction used is itself suspect. This is because the interaction as calculated in (50) includes no short-range (repulsive) part, which might be expected to be significant for broadening by neutral hydrogen or helium, with comparable (relatively low) polarizabilities. Hindmarsh et al (1967) have calculated

the broadening for a parameterized Lennard-Jones potential as given in Eq. (7). The predicted broadening is generally greater with the inclusion of the C_{12} repulsive term and thus in better agreement with the experiments to be described below. However, their analysis depends on experimental values of $\Delta\omega_{1/2}$ and the shift for the determination of the interaction constants C_6 and C_{12} and is ambiguous.

Roueff and Van Regemorter (1969) have attempted to include a short-range component in the interaction

$$V = - \frac{C_6}{R^6} \pm J \tag{67}$$

to allow for an exchange potential at short-range. The exchange term they write as

$$J = J_o r^{\nu} e^{-Ar}$$

where J_o, ν and A depend only on the atomic wave functions. They use this potential to calculate a new ρ_{min} for collisions between ground state radiators and ground state perturbers. Comparison of predicted and experimental line widths for this theory, though, requires calculations for the interaction between excited state radiators and ground state perturbers.

III. EXPERIMENTAL TECHNIQUES

To heat hydrogen or helium to 5000°K at the densities ($\leq 10^{18}$ - 10^{20} cm^{-3}) required for appreciable Van der Waals broadening of the sodium D lines or magnesium B lines poses formidable experimental difficulties. Conventional shock tube methods are ineffective since they rely on a driver gas whose mass density is significantly lower, and hence sound speed significantly higher, than the test gas to be heated. Plasma discharge sources were also ruled out as they generally operate at lower gas densities and produce significant ionization and hence electron densities that would complicate measured line widths with a Stark broadening contribution. It is possible that a discharge source could be looked at during the "after-glow" recombination phase when the electron density was low, but such a method would require a good knowledge of N_e (t). Therefore it was decided to heat hydrogen or helium by adiabatically compressing it with a piston driven by the impulse of a high pressure diaphragm burst. As such, a shock tube was modified and a long series of diagnostic experiments begun to determine the merit of the method and the experimental configuration that best achieved theoretical predictions of the compressed gas conditions. Before describing the techniques for optimum operation finally arrived at,

we present a discussion of an idealized piston-compressor's operation.

A. Piston Compressor Model

The ballistic piston compressor that has been developed to study neutral atom pressure broadening is illustrated diagramatically in Figure 1. The overall design is similar to that of the instrument developed by Lalos and Hammond (1962) to study broadening at pressures of thousands of atmospheres. The chief concern in our work, though, has been to minimize the density (pressure) of the compressed perturbing gas at the astrophysically interesting temperature of 5000°K, since we would like to measure the broadening in hydrogen at $N \simeq 10^{17} cm^{-3}$, typical of the solar atmosphere. The minimum final densities attainable with our final compressor design however, are of order $10^{20} cm^{-3}$ in hydrogen and $\sim 10^{19} cm^{-3}$ in helium. We shall now describe the calculations used to predict final compressed test gas conditions.

With reference to Figure 1 let the pressure and volume of the high pressure driver gas be P_2 and V_2 and the corresponding quantities for the low pressure gas be P_1 and V_1,

respectively. Initial values of these quantities will be designated by the superscript o. Let the origin of the one-dimensional coordinate system be at the end of the test-section (end plug). The total length of the tube is then L; the diaphragm and initial piston position is x_o; the position of equilibrium pressure on the piston is x_e; and the position of the piston at maximum compression is x_m. Given x_o and L, as well as P_2^o, P_1^o and V_1^o, we desire to calculate x_e and x_m and the corresponding final values of P_1, T, and N. Since in actual practice we expect the compression to be sudden, we assume the compression is adiabatic. Assuming that no gas leaks around the piston, we then have

$$P_1 = P_1^o\left(\frac{V_1^o}{V_1}\right)^\gamma = P_1^o\left(\frac{Ax_o}{Ax}\right) = P_1^o\left(\frac{x_o}{x}\right)^\gamma$$

$$P_2 = P_2^o\left(\frac{V_2^o}{V_2}\right)^\gamma = -P_2^o\left(\frac{A(L-x_o)}{A(L-x)}\right)^\gamma = -P_2^o\left(\frac{L-x_o}{L-x}\right)^\gamma \qquad (68)$$

where A is the (constant) cross-sectional area of the tube and γ is the ratio of specific heats. The minus sign on P_2 is needed if we are to refer (L-x) to the same origin as x. In practice, P_1^o is not known exactly as some initial leakage

(and final leackage) around the piston always occurs. The amount of leakage necessary to bring observed and calculated final conditions into agreement is small. Additional design improvements should reduce leakage to a negligible level. To insure the simplest interpretation of actual results, the driver gas and test gas were always the same type (helium).

The equation of motion for the piston of mass m may simply be written as:

$$m\ddot{x} = \frac{md^2x}{dt^2} = AP_1 - AP_2 \tag{69}$$

This equation is known to be not entirely exact as it neglects friction forces on the piston. While on some actual shots the deviation of observed from calculated final gas conditions could be attributed to frictional losses, the present (and proposed) piston compressor design is such that these losses should be negligible.

Eq. (69) may then be written

$$\ddot{x} = C_1 x^{-\gamma} + C_2(L-x)^{-\gamma} \tag{70}$$

$$C_1 = \frac{P_1^o}{m} x_o^{\gamma}, \quad C_2 = \frac{P_2^o}{m} (L-x_o)^{\gamma}$$

Multiplying this equation by the piston velocity $\dot{x}$ gives

$$\dot{x}\ddot{x} - C_1\dot{x}\, x^{-\gamma} - C_2\dot{x}(L-x)^{-\gamma} = 0$$

which may be integrated once with respect to time:

$$\frac{1}{2}\dot{x}^2 + \frac{C_1}{\gamma-1} x^{1-\gamma} + \frac{C_2}{\gamma-1} (L-x)^{1-\gamma} = K_1$$

$$= \frac{C_1}{\gamma-1} x_o^{1-\gamma} + \frac{C_2}{\gamma-1} (L-x_o)^{1-\gamma} \qquad (71)$$

where K_1 is an integration constant fixed by the initial condition that $\dot{x} = 0$ when $x = x_o$. Eq. (71) could be transformed to the form of the general elliptic equation (Davis, 1962) if the exponent were an integer instead of its actual value of 5/3 (helium) or 7/5 (hydrogen). As such, the equation appears to be unsolvable, except by numerical techniques.

However, we can readily solve eqs. (70) and (71) for

x_e and x_m, respectively, and these are the quantities of real interest. Eq. (71) suggests that the actual piston motion will have a damped oscillatory character. The equilibrium position x_e will be the point about which the piston oscillates. It is determined from the condition that at x_e the net force vanishes

$$\left[\frac{x_e}{(L-x_e)}\right]^{-\gamma} = \frac{C_2}{C_1}$$

and so

$$x_e = L\left[1 + \frac{C_2}{C_1}^{1/\gamma}\right]^{-1} \tag{72}$$

The expression for the position of maximum compression, x_m, is obtained from (71) by noting that at x_m, $\dot{x}$ vanishes. Then

$$\frac{C_1}{C_2} = \frac{(L-x_o)^{1-\gamma} - (L-x_m)^{1-\gamma}}{x_m^{1-\gamma} - x_o^{1-\gamma}}$$

or

$$x_m^{1-\gamma} = \left(\frac{C_2}{C_1}\right)\left[(L-x_m)^{1-\gamma} - (L-x_o)^{1-\gamma}\right] + x_o^{1-\gamma}$$

and so

$$x_m = \frac{C_2}{C_1}\left\{(L-x_m)^{1-\gamma} - (L-x_o)^{1-\gamma}\right\}^{1/1-\gamma} \tag{73}$$

This equation still contains x_m on the right-hand side. However, we note that in actual fact x_m must be very small compared to L for large P_2^o and small P_1^o. This follows both intuitively and from the fact that $x_m < x_e$ and eq. (72). Thus we may approximate (73) by letting $(L - x_m) \simeq L$, and so

$$x_m \simeq \left\{\frac{P_2^o (L-x_o)^\gamma}{P_1^o x_o^\gamma}\left[L^{1-\gamma} - (L-x_o)^{1-\gamma}\right] + x_o^{1-\gamma}\right\}^{\frac{1}{1-\gamma}} \tag{74}$$

This result for x_m may then be substituted back into eq. (73) and several such iterations carried out. In practice this was done on the computer, and the convergence was rapid. We note in passing that the expressions (73) and (74) could also

have been obtained from eq. (69) by arguing that the work done in compressing the test gas must equal the negative of the work done by the expanding driver gas, and thus x_m is independent of the piston mass in this approximation.

The computer program written to solve eqs. (73) and (74) for the final compressed gas volume, $V = Ax_m$ was also used to give the final values of the pressure, temperature, and density from the usual adiabatic relations

$$P = P_1^o \left(\frac{x_o}{x_m}\right)^\gamma$$

$$T = T^o \left(\frac{P}{P_1^o}\right)^{\frac{\gamma-1}{\gamma}} \qquad (75)$$

$$N = \frac{P}{kT}$$

It is clear from eqs. (75) that a given temperature T may be achieved at the lowest final densities N for a given P_1^o and P_2^o if the test gas is monatomic with $\gamma = 5/3$ instead a diatomic gas with $\gamma = 7/5$. Therefore, and for safety reasons in developing operating techniques with the new piston compressor, all experiments have been done in helium. However, γ may still be less than 5/3 if the final

temperatures and densities are sufficient for significant ionization, in which case $\gamma \rightarrow 1$. The agreement of the final gas conditions predicted from eqs. (74) and (75) is then dependent on the concentration of low-ionization potential impurity or injected sample atoms, as well as on the values of T and N. The experimental measurements reported below involved $T \leqslant 5000°K$ and $N \simeq 10^{20} cm^{-3}$. With test sample (Na) concentrations of the order of 1%, and impurity concentrations certainly much less, the Saha calculations we shall discuss predicted of the order of 1% ionization. The additional energy going into ionization in this case requires the compression ratio $(V/V_o) \simeq 68$ be increased by a factor of 1.05 to 71.5. Thus γ would be reduced to approximately 1.655 (from 1.667). In view of the assumptions made, we may conclude that for the experimental conditions of interest the depression of γ due to ionization is probably negligible. Frictional losses and piston leakage in the existing piston compressor are more important in effectively reducing γ and the efficiency of the compression.

The results of some representative calculations of expected final compressed gas conditions for helium and hydrogen are presented in Figures 3-8. In each case, x_m,

T, and N are plotted as functions of the initial fill pressure P_1^o at two different initial driver pressures P_2^o of 50 psi and 125 psi. The calculations for helium (Figs. 3 and 4) and for hydrogen (Figs. 5 and 6) were done using the dimensions of the existing piston compressor in eqs. (73) and (74); that is, x_o = 365 cm and L = 460 cm. The final two cases (Figs. 7 and 8) considered were again for hydrogen but with L = 385 cm so that the driver section was only 20 cm long. Since for a given ratio of driver to test section volume, $x_o/(L-x_o)$, x_m scales linearly with x_o, the final case demonstrated that experiments in hydrogen require a longer tube with a shorter driver section to insure a reasonable volume ($x_m \simeq 1$ cm) of test gas at $T \simeq 5000°K$ and $N \simeq 10^{20}\,cm^{-3}$ in which to measure Van der Waals broadening. Note that the calculations for hydrogen were done with an initial temperature $T_o = 400°K$, whereas for helium $T_o = 300°K$. Since lower final densities may be achieved for a given final temperature (5000°K) and volume ($x_m \simeq 1$ cm) with higher initial temperature, $T_o = 400°K$ would seem necessary for experiments in helium if we hope to make confident extrapolations of measured line widths to solar photospheric densities $N \approx 10^{17}\,cm^{-3}$. Actual operating values of P_1^o and P_2^o were chosen in accordance with the results shown in Figs. 3

and 4 (and many others like them) for T_o = 300°K and different P_2^o such that T ≃ 5000°K (indicated by a circle on each curve) and $x_m \geq 1$ cm. The latter requirement was imposed to minimize boundary layer problems and possible inhomogeneities, and in fact (Figs. 3 and 4) $x_m \simeq 5.4$ cm in all cases in helium at 5000°K. The proper choice of P_1^o and P_2^o then could be made to select final densities over the approximate range $5 \times 10^{19} < N_{He} \leq 5 \times 10^{20}$ cm^{-3}.

B. Diagnostics

In this section we shall describe the diagnostic methods developed to measure the actual values of P, T, and N in the test gas and the line widths themselves on a time-resolved basis.

The gas pressure was monitored continuously with a quartz piezo-electric transducer mounted in the end-plug (see Fig. 1). The charge developed across the crystal was amplified by a charge amplifier and displayed on an oscilloscope. The pressure measured was in fact the actual pressure since the transducer responds both to the gas pressure in the boundary layer and to the momentum transfer of the

piston associated with the heat flux.

Temperatures were measured at any prescribed time during maximum compression (~ 100 μsec) and associated light emission by the line reversal method (Parkinson and Reeves, 1964). By this technique, a high intensity flash lamp (FX-12; see Fig. 1) is triggered during the light emission, and the intensity transmitted at the wave length of the line in question (Na-D) is compared with the intensity transmitted by the uncompressed gas for a measure of the emissivity of the radiating gas. From this a black-body temperature can be calculated directly, having calibrated the system with a standard tungsten lamp of known spectral temperature and emissivity. Since the method depends on any loss of FX-12 intensity being due to actual absorption in the line, a control monochromator was also used to monitor the FX-12 intensity transmitted in the continuum or (on some occasions) in the core of another comparison line. This precaution was taken to discriminate against refraction losses of FX-12 intensity and provided a check on the homogeneity of the test gas. Simultaneous comparison temperatures at the core of a line (e.g. Ba II 4554 Å, present as an impurity in early work) other than that of interest (Na-D) also provided

a check on LTE conditions and, more importantly, could provide a check on the extent of the suspected Na boundary layer. Such comparison line center temperature measurements generally agreed to within ~200°K, while monitoring continuum FX-12 intensities near the line revealed that refractive effects were sometimes present at maximum compression and that the most reliable experimental conditions occur just before this peak.

Neutral perturber gas (helium) densities and electron densities were measured by a two-wave length Fabry-Perot interferometer technique (see Fig. 2). As the piston compresses the gas, the index of refraction changes with increasing particle density and the resulting continuous change in optical path length between the two stationary Fabry-Perot flats on either side of the test-section appears as a series of fringes. The number of these fringes at any time may then be used to calculate the corresponding density. Because of dispersion, the changes in index of refraction for a given increment in neutral gas density is much greater at 6328 Å than at 3.39μ whereas at the infra red frequencies the change in the index of refraction due to significant electron densities is greater than for visible wavelengths. Thus the 6328 Å fringe count is used to infer the neutral (He) density and the 3.39μ fringe count

the electron density. The two wave lengths named were chosen because they are the two strongest lines available from a helium-neon laser. As both lines arise from transitions from a common upper level, the He-Ne laser may be operated (with the proper mirrors) at only one wave length for maximum power. Thus two separate He-Ne lasers were used.

The number of fringes m observed for a change $\Delta n = |n-1|$ in the index of refraction is simply

$$m = \frac{2|n-1|d}{\lambda_o} \tag{76}$$

where d is the fixed distance between the F-P flats, which are illuminated by the two laser beams brought into coincidence by a beam-splitter to normal incidence. In actuality, d is just the linear dimension of the test gas confined in the piston-compressor test section since only over this distance (5 cm) does the index of refraction change. The difference in the index of refraction from unity is linearly dependent on the neutral gas density

$$\frac{\Delta n}{\Delta n_{STP}} = \frac{N}{N_{STP}} \tag{77}$$

For helium, $\Delta n_{STP} = (n-1)_{STP} = 3.5 \times 10^{-5}$, and $N_{STP} = 2.68 \times 10^{19} cm^{-3}$, so substituting (77) into (76) we obtain

$$N_{He} = 4.85 \times 10^{18} m_{6328\ \text{Å}}\ cm^{-3} \tag{78}$$

where we used $\lambda_o = 6328$ Å. The same derivation for the 3.39μ laser beam would give simply a factor of $33.9/6.328 \simeq 5.35$ fewer fringes m for any helium density N_{He}.

The contribution of the electrons to the refractive index is given by the well-known relation, assuming the collision frequency $\nu_{coll} << \nu$ **

$$n^2 = 1 - \frac{\nu_p^2}{\nu^2} \tag{79}$$

where the plasma frequency ν_p is

$$\nu_p = 8.97 \times 10^3 N_e^{1/2} \tag{80}$$

** We note that by Lorentz theory of pressure broadening discussed in the first part of Section II, $\Delta\nu \approx \nu$coll:. Thus even for Na-D (5890 Å) broadened to $\Delta\lambda \simeq 10$ Å, $\Delta\nu = \frac{c\Delta\lambda}{2} \simeq 8.7 \times 10^{12} << 8.85 \times 10^{13} \simeq \nu_{3.39\mu}$ and (79) may be used.

Since $n+1 \simeq 2$ we may make the approximation

$$n^2 - 1 = (n-1)\ (n+1) \simeq 2(n-1) \tag{81}$$

and thus write, using (79) and (80),

$$2|n-1| \simeq \frac{8.06 \times 10^7 N_e}{\nu^2} \tag{82}$$

Substituting this result into Eq. (76) and evaluating for $\lambda_o = 3.39\mu = \nu/c$ we find

$$N_e = 6.62 \times 10^{15} m_{3.39\mu} cm^{-3} \tag{83}$$

Once again, the contribution at the other wavelength (6328 Å) would give a factor

$$\frac{\nu_{6328\ Å}}{\nu_{3.39}} \cdot \frac{\lambda_{6321\ Å}}{\lambda_{3.39\mu}} = \frac{\lambda_{3.39\mu}}{\lambda_{6328\ Å}} = 5.35$$

fewer fringes for any given electron density N_e.

Aside from the factor 5.35 difference in the number of fringes at each wavelength, the possible contribution of N_e to $m_{6328\ \text{Å}}$ and N_{He} to $m_{3.39\mu}$ was further discriminated against by the gross difference in the total time interval in which the respective fringes could be expected. That is, while the total fringe count $m_{6328\ \text{Å}}$ is accumulated during the entire compression time or piston travel time (~ 25msec), the fringe count $m_{3.39\mu}$ is expected to significantly increase (if there are electrons) just during peak compression and light emission times (~ 200 μsec).

The actual line profiles were measured with a rapid-scanning Fabry-Perot interferometer (Cooper and Greig, 1963). As illustrated in Fig. 1, this instrument views the light emission along optical axis for temperature measurement at 90° from the axis of the density measuring Fabry-Perot. Light from the compressed gas was directed into a plane parallel beam along the interferometer axis via a beam splitter, aperture, and lens. The collimated beam out of the interferometer was re-focused onto the entrance

slit of a monochromator, and the intensity in the line of interest recorded on an oscilloscope as the output of a photomultiplier at the monochromator exit slit. The scanning of a given wavelength region, chosen (via the monochromator) to include the line of interest, was done by continuously varying the separation d of interferometer flats. This variation was in fact accomplished by mounting one of the flats on a piezoelectric crystal (barium-titanate) driven at its resonant frequency of ~ 15 kc. so that the etalon position oscillated about a fixed separation d_o and the same wavelength interval was rapidly re-scanned many times.

This intensity distribution of the ideal fringes of a Fabry-Perot is described by Airy's formula (Born and Wolf, 1959)

$$A(\alpha) = \frac{T^2}{(1-R)^2} \left\{ 1 + \frac{4R}{(1-R)^2} \sin^2 \frac{\pi\Delta}{\lambda} \right\} \qquad (84)$$

where R and T are the reflection and transmission coefficients of each etalon and Δ = 2nd cosi (optical retardation) with n = refraction index and i = angle of incidence. Transmission maxima must then occur when the $\sin^2$ term vanishes, i.e. when $\Delta = m\lambda$, where m is an integer known as the order. Thus if Δ = const., the equivalent wavelength change

corresponding to $\Delta m = \pm 1$ is

$$\Delta\lambda_1 = \frac{\lambda^2}{\Delta} \simeq \frac{\lambda^2}{2d} \tag{85}$$

where we have set $n \simeq 1$ (air) and $i = 0°$ (normal incidence). This wavelength interval is known as the free spectral range (hereafter often abbreviated FSR) and sets the scale for the maximum bandwidth (i.e. line width) resolvable into fringe orders m with the interferometer. Because in each free spectral range the condition $m\lambda = 2d$ must be satisfied, it follows that

$$\frac{\Delta\lambda}{\lambda} = \frac{\Delta d}{d_o} \tag{86}$$

where d_o is the median separation of the etalons. Thus within a free spectral range the change in wavelength $\Delta\lambda$ accepted by the first focusing aperture (and hence the interferometer) is directly proportional to the change in etalon separation Δd. Each time the separation changes by $x/2$, the order m changes by one and the scan is repeated.

Cooper and Greig (1963) show that the separation d of the two Fabry-Perot flats is

$$d = d_o + y_o \sin \frac{\pi c t}{\ell} \qquad (87)$$

where y_o is amplitude of oscillation of the resonant vibrator (barium titanate) with length ℓ, and sound speed c. Then solving for $\Delta d/\Delta t$ and putting $\Delta d = \lambda/2$, the minimum time required to scan the free spectral range is

$$\Delta t_{min} = \frac{\lambda}{4\pi y_o f} \simeq 0.1 \ \mu\text{sec.}$$

for λ in the visible and resonant frequency $f \simeq 15$ kc and y_o determined by the breaking strain of the varium titanate. Since the velocity of the moving flat predicted by Eq. (87) is linear to within 1% over the center 9% of the half-period (Cooper and Greig, 1963), the linear time axis of the oscilloscope, on which the several orders of the central fringe (as seen by the monochromator) are displayed, is also the linear wavelength scale. Thus the experimental line width could be read directly from the oscilloscope picture, knowing the free spectral range (Eq. (85)) from a measurement

of d_o with a travelling microscope.

The resolution possible for such a line width measurement is determined by the instrument profile half width $\Delta\lambda$ and is generally expressed in terms of the finesse η

$$\eta = \frac{\Delta\lambda_1}{\Delta\lambda} \tag{88}$$

The contributions to the finesse from the etalon reflectivity surface defects, and finite scanning aperture width are discussed in detail by Chabbal (1953). Surface defects (i.e. departures from flatness and parallelism) of the etalons are the chief limitations on finesse, which in practice (i.e. for $\lambda/50$ flats) doesn't exceed 25.

From Eq. (88) we see that since the instrument width is $1/\eta$ of $\Delta\lambda$, line widths may be measured to an effective accuracy of about $\pm$ $1/2\eta$. The actual half width of the Lorentzian profile of the pressure broadened line of interest must be determined from the measured Voigt profile's half width by a deconvolution of the measured instrumental Voigt profile. The data are further complicated by the fact

that in general ($\eta \simeq 10$) the measured profiles are overlapping. Fortunately, Day (1967) has calculated extensive tables for just this purpose of extracting the Lorentzian half width from measured overlapping Voigt profiles, thus considerably simplifying the reduction of the data reported below.

C. Operating Procedure

After considerable experimentation, the operating procedures for optimum self-consistency and repeatability of the final compressed gas conditions was established. With the tube initially filled with helium at pressure P_1° = 10 mm. Hg and an aluminum sheet diaphragm chosen to burst at (typically) P_5° = 130 psi, the helium driver gas was brought up to this pressure. When the diaphragm bursts, the driver gas funneled through the piston mount (see Fig. 1) into the center of the piston, thus minimizing any initial leakage of driven gas around the piston. The sound of the bursting diaphragm was converted by a piezo-electric microphone mounted solidly on the tube into a pulse used to trigger the oscilloscope beam displaying the pressure transducer output. The time scale used for this beam was

typically 10 msec/cm, as the (~ 100 gm) piston required about 30 msec to reach x_m and maximum compression. The pressure transducer's charge amplifier was set at a gain sufficient to give a pulse of several volts at P_1^{max}, and this signal was itself used to trigger the oscilloscope's second time base to record the output of the two temperature measurement monochromators. Due to the usually fast rise time of the pressure pulse ($\leq$ 1 msec), the exact trigger level for the monochromator's oscilloscope record was not critical and was usually set at ~ 1v. The time scale for these two beams was 200 μsec/cm., since the total duration of light emission was typically < .6 msec. After several trial shots, the "exact" timing of the light emission with respect to the chosen trigger level on the pressure pulse could be ascertained, and the timing of the FX-12 flash lamp was then appropriately adjusted by means of an independent electronic delay unit. This delay was adjusted so that the FX-12 fired just before maximum light emission.

This same FX-12 trigger pulse was also brought to trigger the sweep of two other oscilloscopes - one to record the rapid scanning Fabry-Perot output on a 5 μsec/cm time base and the other to record both the fringes at 6328 Å and at

3.39μ from the N_{He} - and N_e - measuring Fabry-Perots, respectively, on a 200 μsec/cm time base. Thus the line widths were measured simultaneously with the temperature determination, while the total laser fringe counts were compared from this time until the end of light emission for the estimate of N_e. Still another oscilloscope, triggered by the initial diaphragm burst, displayed on two sequential time bases (2 μsec/cm and 1 μsec/cm) the total fringe count at 6328 Å from the time of the diaphragm burst to peak compression for the determination of N_{He}. As this record actually extends on to perhaps 5 msec after peak compression, the fringe count during decompression provided a comparison check.

A small sample of finely powdered non-deliquescent salt of the particular element whose pressure-broadened spectrum is to be studied may be puffed into the initially evacuated test section with the supporting helium gas. Observations of the settling time of the sample particles have shown that there is typically a period of several seconds during which the piston can be fired to insure maximum homogeneity of the sample in the test gas. Such a sample injection technique is, of course, essential for line profile measurements of most elements of astrophysical interest, such as Mg, Ca, or

Si which wouldn't normally be present in the tube as impurities. However, it was found that enough Na was present as an impurity in the test section and on the piston itself that additional injection (of Na SbO_3) was unnecessary. Particularly since the Na-D line studied is a resonance transition, it was found that upon injecting additional sodium salts, the resulting cool boundary layer was severe enough to cause appreciable self-reversal in the line core, thereby confusing any measurements of the width. With no sample injected though, the Na boundary layer appears tolerable even though the Na must come from the walls. This is particularly true for shots with maximum pressure pulse rise times and hence rates of heating and mixing. The pressure pulse rise time in turn is dictated by the leakage of compressed gas around the piston and hence the piston fit. Ultimately the best way found to tighten the piston fit (when needed) for each shot was to compress the piston in a press thereby flaring out the leading and trailing sealing edges.

The alignment of the two coincident beam density-measuring laser Fabry-Perot interferometers was difficult in that the reflected beams must not re-enter the (6328 Å) laser to prevent excitation of spurious modes. However, the rapid-scanning Fabry-Perot was even more critical as its alignment

is subject to thermal and mechanical effects and is stable for at most only several minutes. Therefore, when all other preparations had been made to fire a shot, the calibration scan of a reference Na-lamp was taken at 5890 Å, and the shot fired as soon as possible thereafter. If possible a second calibration scan was made of the reference lamp after the shot for comparison purposes. The calibration scans are essential, of course, for the measurement of the finesse or instrument profile of the interferometer. Finally, we note that in practice the entrance and exit slits of the monochromator (Fig. 2) for this interferometer were kept wide in anticipation of a (red) shift from 5889 Å of the experimental profile. Unfortunately, this experiment is not at present equipped to measure quantitatively this shift.

IV. EXPERIMENTAL RESULTS

In practice, carrying out the operating procedure outlined above, which itself was the result of many other methods attempted, proved to be quite difficult. Many unforeseen problems arose: structural failures of the piston compressor test section, countless problems with piston fit, low frequency laboratory vibrations giving misleading density interferometer fringe counts, and many more. However, these problems were all solved, or at lease minimized, and we may summarize our results as follows.

The first measurements obtained were values of the pressure, temperature, and neutral density at (approximately) maximum compression. These values were found to be usually quite self-consistent, i.e. they satisfied the ideal gas relation $P = NkT$. The discrepancies amongst these values could usually be explained by either a lack of exact simultaneity in all three measurements or by a lack of experimental resolution, particularly for the pressure measurement. These final experimental values of P, T, and N_{He} could generally be fit to a set of calculated curves

(e.g. Fig. 4) for an ideal helium piston compressor with the actual driver pressure P_2^o for a proper choice of P_1^o. This adjusted value of the initial test gas pressure was greater than the actual value of P_1^o used and provided a measure of the initial piston leakage as well as probable (final) piston leakage of the compressed gas. That final piston leakage must probably occur was indicated by the fact that on some shots the piston partially blocked the windows, giving an upper limit on x_m (Fig. 4).

The experimental capability to measure electron densities was not acquired until after much of the initial work had been done, and thus comparisons of estimates of N_e with the Saha values predicted for measured P, T, and N have only recently been possible. The Saha calculations were carried out using the H.C.O. computer program "EXCIT 6", which calculated ionization equilibrium at sodium concentrations ranging from .1% to 5% and over the range of experimental pressures (300 psi - 3000 psi) and temperatures (~2500°K - 6000°K). The experimental results were quite consistent with these calculations. That is, a typical shot for which Na sample was injected with the helium gave (5 fringes at 3.39), $N_e \sim 3.3 \times 10^{16} cm^{-3}$ for a measured $P \simeq 700$ psi, $T \simeq 3500$ K, and $N_{He} \simeq 1.0 \times 10^{20} cm^{-3}$. These values are all

almost exactly correct for the Saha calculation with a Na concentration of 5%. Although the sample injection technique does not permit an exact knowledge of the sample concentration in the test gas, a 5% concentration seems very reasonable in light of past shock tube work. As mentioned above, however, the Na-D line profile measurements were made without injecting Na in a powdered salt. The 3.39 μ fringes during light emission for these shots were similar in relative timing but about 4-5 times less dense than the corresponding fringes at 6328 Å. We conclude then that they represent for the most part the changes in the neutral helium density and that (see eq. (83)) $N_e \leqslant 10^{16} cm^{-3}$ for these shots with measured temperatures in the range $2650°K \leq T \leq 4500°K$, and densities $10^{20} \leqslant N_{He} \leqslant 3.2 \times 10^{20}$. The Saha calculations again show that these conditions are nearly self-consistent with those calculated for Na concentrations of $\leqslant .1\%$, which seems not unreasonable for an impurity like Na so easily introduced even by handling the piston.

The experimental results of the measurements of the Na-D (5889 Å) width in helium are given below and in the log-log plot (Figure 9) of half-width as a function of

helium density. In plotting these data (Figure 9) we have used the last two columns of Table 1. The error bars on the adopted density are equal in length to $(N^{inf} - N^{m})$, and the (minimum) errors in the widths are at least $\pm 1/2\eta$, where η is the finesse as discussed above. The widths have all been normalized to the astrophysically interesting $T = 4500^{\circ}K$, which was the approximate measured T^{m} for data (III). The normalization assumes a (weak) temperature dependence of $\Delta\lambda$ as given by our impact approximation result, eq. (55).

It is unfortunate that the data all fall within the interval $10^{20} \lesssim N \lesssim 3 \times 10^{20}$ but this is a consequence of the departures of our piston compressor from the ideal behavior discussed above. Of the six data groups obtained, only three are actual measured widths; the last three represent lower limits dictated by the particular free spectral range of the rapid scanning Fabry-Perot. The length of the upward pointing arrow (Figure 9) on these three lower limits indicates the degree to which fringes (i.e. line profiles) are lacking; i.e. the data of (VI) shows no evidence of fringes while (IV) (especially), and

(V) both show a vague suggestion of profiles that might have been measured at larger F.S.R.

A straight line with unit slope may (cautiously) be drawn through data points (I), (II), and (III). This would be an important confirmation of the maintenance of a linear relationship between half-width and perturber density at these high densities, and one would be tempted to extrapolate back to the photospheric densities of $N \simeq 10^{17}\,cm^{-3}$ and thus infer (from the ratio of the dipole polarizabilities of helium and hydrogen) the values of the solar Van der Waals damping constant (see Conclusions below). The experimental data and their linear interpretation finally provides a check on the result of our impact approximation calculation for the width, eq. (55a), and the similar result obtained by Griem (1964), which differs only by a factor 3/2 under the brackets.

A computer program was used to evaluate Griem's result for Na-D in He over the range of experimental temperatures. For purposes of comparison with the linear interpretation of the data in Figure 9, the result for 4500°K and broadening of the upper state only was $\Delta\lambda_{Griem} = 1.347$ Å at $N = 10^{20}$

TABLE 1: EXPERIMENTAL HALF WIDTHS OF Na (5889 Å) IN He

Data No.	Measured Lorentzian Half-width $\Delta\lambda_m$	Measured Temperature T^m	Measured Pressure P^m	Inferred Helium Density N_{He}^{inf}	Measured Helium Density N_{He}^m	Adopted He Density $N_{He} = \frac{(N^{inf} + N^m)}{2}$	Normalized (4500°K) Half-width $\Delta\lambda_p = \Delta\lambda_m \left(\frac{4500}{T^m}\right)^{.3}$
(I)	9.5 ±.9Å	3500°K	1250 psi	1.8×10^{20} cm^{-3}	1.6×10^{20} cm^{-3}	1.7×10^{20} cm^{-3}	10.4 ± 1 Å
(II)	12.6±1.2Å	$\gtrsim$4500°K	$\sim$2500 psi	$\lesssim 2.5 \times 10^{20}$ cm^{-3}	$\gtrsim 1.5 \times 10^{20}$ cm^{-3}	2.1×10^{20} cm^{-3}	12.6 ± 1.2 Å
(III)	12.25±1.75Å	2650°K	1320 psi	2.5×10^{20} cm^{-3}	1.9×10^{20} cm^{-3}	2.2×10^{20} cm^{-3}	14.3 ± 2 Å
(IV)	>5.5 Å	2500°K	$\lesssim$1000 psi	$< 2 \times 10^{20}$ cm^{-3}	1.0×10^{20} cm^{-3}	1.25×10^{20} cm^{-3}	>6.5 Å
(V)	>6.9 Å	3187°K			1.50×10^{20} cm^{-3}	1.50×10^{20} cm^{-3}	>7.7 Å
(VI)	>8 Å	3510°K	1870 psi	2.65×10^{20}	2×10^{20} cm^{-3}	2.4×10^{20} cm^{-3}	>8.65 Å

instead of the value $\Delta\lambda_p = 6.1$ Å from Figure 9. Thus our experimental result, if indeed linear, gives 4.5 times the broadening predicted by Griem at $N = 10^{20}$. The same computer evaluation gave for our expression eq. (60), the limiting density value

$$N_{4500°} << 3.18 \times 10^{21} cm^{-3}$$

and thus we may tentatively assume that our experimental results are still within the limits of the impact approximation. Recalling eq. (66), we have additional reason to believe that the experimental $\Delta\lambda_p$ vs. N_{He} curve should be linear as opposed to quadratic in N.

The discrepancy of Figure 9a with the impact approximation result shown in Figure 9b may be lessened somewhat if the same equation (55a) is applied to the lower level of the transition. Then if the broadening of both levels is naively added, the theory gives $\Delta\lambda_{Griem} = 2.427$ Å at $N = 1 \times 10^{20}$ for a discrepancy of 2.5. There is certainly justification for considering the broadening of the lower level, and Traving (1959) estimates that its proper inclusion may

increase the effective interaction constant by a factor of 5 to 10. However, it is unlikely that we may apply the same theory that gave eq. (55) (since in going from eq. (31) to (32) we neglected one level) to both states and simply add the broadening. Therefore our final remarks will be restricted to comparisons with the one-level calculation, and we adopt the value

$$\Delta\lambda_p = \frac{\lambda_o^2 \omega_{\frac{1}{2}-\frac{1}{2}} \times 10^8}{2\pi c} = 6.1 \text{ N} \times 10^{-20} \text{ Å} \qquad (89)$$

as the result of our measurements for the half width of Na (5890 Å) in He at 4500°K.

This measured half-width may be entirely (to within experimental accuracy) attributed to pressure broadening by neutral helium atoms. That is, for the measured $N_e \leqslant 10^{16} cm^{-3}$, Griem (1964) gives the Stark broadened half-width of only .022 Å. Also, at T = 4500°K the Gaussian profile Doppler half-width in angstrom units is

$$\Delta\lambda_G = \lambda_o \left[\frac{2kT\ell n2}{mc^2}\right]^{1/2} \times 2 \times 10^8 \simeq .059 \text{ Å} \qquad (90)$$

Finally, the resonance broadening of Na-D may also be

neglected in view of the fact that $N_{Na} << N_{He}$.

V. CONCLUSIONS

First we should like to compare our result given in (89) with other experimental determination of Na-D (λ 5890) broadening in He, notably that of Behmenburg (1964). Behmenburg found the broadening to be greater by a factor of 2 than the Van der Waals prediction at $N_{He} = 3 \times 10^{18}$ and $T = 2650^{\circ}K$. His measurements were restricted to approximately these temperatures and densities, and were performed using a sodium flame into which various perturbing gases were mixed. The results for helium are ambiguous for several reasons, however. First, it is not clear (Ch'en and Takeo, 1957) how important the Doppler broadening is under flame conditions. Second, and more important to the data analysis, the questions of complete mixing of the He and Na atoms as well as the broadening contributions of impurity gases necessarily arise. Behmenburg points out that for his helium measurements, only 75% of the flame gases were He, the remaining 25% being largely CO_2, CO, H_2O, and OH. It is quite possible, then, that Behmenburg's results and our measurements, that would suggest a factor of 4.5 discrepancy with theory at these densities, are in

agreement.

For purposes of eventually constructing more adequate theories of the broadening at the densities measured here, it may be useful to evaluate (by the existing theory) the experimental value of the interaction constant, C_6. To do this, we shall equate our result, eq. (89), with the impact approximation, eq. (59), written with the 3/2 factor (Griem) to facilitate comparison with the calculated widths quoted above

$$\Delta\omega_{\frac{1}{2}-\frac{1}{2}} = \frac{\pi c}{\lambda_o^2} \times 6.1N \times 10^{-28} = \pi N \left[\frac{9\pi C_6^{exp}}{16\hbar}\right]^{2/5} \bar{v}^{3/5}$$

Solving then for the experimental value of the Van der Waals constant, C_6^{exp}

$$C_6^{exp} = \frac{16\hbar}{9\pi}\left[\frac{6.1 \times 10^{-28} c}{\lambda_o^2\ \bar{v}^{3/5}}\right]^{5/2} \tag{91}$$

$$\simeq 3.23 \times 10^{-59} \text{ erg cm}^6$$

where we have substituted $\lambda_o = 5890$ Å, and $T = 4500\,^{\circ}K$ into eq. (53) for $\bar{v}$. The theoretical value of C_6 predicted by eq. (50) is

$$C_6^{theory} = e^2 \alpha_{He} \langle r^2_{Na} \rangle \simeq 5.23 \times 10^{-59} \text{ erg cm}^6 \tag{92}$$

where we have used the value for the helium dipole polarizability

$$\alpha_{He} = 1.384\, a_o^3 \simeq 2.05 \times 10^{-25} \text{ cm}^3 \tag{93}$$

For consistency, we should have used this more accurate value for α_{He} in evaluating (91) instead of the approximation of eq. (57)

$$\alpha_{He} \simeq \frac{\hbar^2 e^2}{mE^2} \simeq 2.8 \times 10^{-25} \text{ cm}^3 \tag{94}$$

used in the derivation of eq. (59) and hence (91). Thus we divide the result of (91) by the ratio of these two polarizabilities, 1.36 for the more "accurate" experimental value

$$C_6^{exp} \simeq 2.37 \times 10^{-57} \text{ erg cm}^6 \qquad (95)$$

This value differs from (92) then by ratio of the observed to calculated broadening to the 5/2 power, $(4.5)^{2.5}$. It is interesting to note that the inclusion of this better value for α_{He} given (93) just about exactly accounts for the 3/2 discrepancy between our impact approximation result eq. (55) and that given by Griem (1964). We note that our result (95) is about seven times larger than the value Hindmarsh *et al* (1966) give for Behmenburg's work.

We conclude by noting that for the broadening of Na (5890 Å) in neutral hydrogen, these measurements in helium suggest a larger discrepancy with the widths calculated by eq. (55). This would be of the order

$$\Delta\lambda^{exp}_{H-Na} \sim \left(\frac{\alpha_H}{\alpha_{He}}\right)^{2/5} \Delta\lambda^{exp}_{H-Na} \simeq 2.14\Delta\lambda^{exp}_{He-Na} \qquad (96)$$

which would suggest a factor of ≥ 8 discrepancy with the theoretical estimates used (Griem, 1964) in stellar atmospheres work to date. The implications of this would be great indeed as it would necessitate assigning the line (wing) formation regions for the solar Fraunhoffer D-lines to higher layers of lower (by a factor of ≥ 8) hydrogen density. However, such a quantitative prediction is still premature and actual broadening measurements in neutral hydrogen must be made as the actual interaction potential for both He-Na (especially) and H-Na systems is most certainly not just Van der Waals, but at least Lennard-Jones (eq. (7)). In fact a complete specification of the interaction must include an overlap of the perturber and emitter wave functions, which we neglected at the outset in favor of the simple classical path approximation.

A more accurate series of He-Na measurements (at lower densities) is needed to establish the linearity suggested by our measurements and thus remove the uncertainty in extrapolating over several orders of magnitude of the

perturber density. Towards this end, and in hopes of measuring the broadening in hydrogen and possibly even the resonance broadening of Lyman-α, a new much longer piston compressor is being built. It is hoped that the work reported here has at least established some of the groundwork for these future investigations.

VI. ACKNOWLEDGEMENTS

This work was begun with Dr. D.D. Burgess, who first suggested the piston compressor technique as a means of measuring Van der Waals widths in hydrogen and eventually the resonance broadening of Lyman-α. To him I owe a great deal; for encouragement at the outset, for instruction in many experimental methods, and for many profitable discussions of line broadening theory. I should also like to thank Prof. A. Dalgarno, who read the manuscript and made several useful suggestions.

Special thanks are also due to Mr. Les Weir and his staff of the H.C.O. Model Shop who carried out the seemingly endless engineering modifications of the piston compressor. Particular gratitude is due Mr. A. Val Puopolo for his tireless efforts at designing and machining teflon pistons.

Finally I wish to thank Dr. W.H. Parkinson for his enthusiastic support of this project, which was founded by NASA Grant NGL-22-007-006 and the Office of Naval Research, contract number N00014-67-A-0298.

REFERENCES

1. Baranger, M., Atomic and Molecular Proecesses, Bates, D.R., ed., Academic Press, New York, p. 503, 1962.

2. Baranger, M., Phys. Rev., 111, 485 (1958).

3. Behmenburg, W., JORST, 4, 177, 1964*. (Exptl. Results)

4. Bethe, H.A., Salpeter, E.E., Quantum Mechanics of One and Two Electron Atoms, Academic Press, New York, p. 17, 1957.

5. Born, M. and Wolf, E., Principles of Optics, Pergammon Press, New York, 1954.

6. Bracewell, R.M., The Fourier Transform and Its Applications, McGraw Hill, New York, 1965, p. 20.

7. Burgess, D.D., Lecture Notes, 1967.

8. Callaway, J. and Bauer, E., Phys. Rev., 148, A1072 (1965).

9. Cayrel, G., and Cayrel, R., Ap.J., 137, 462, (1963).

10. Chabbal, R., J. Rech. C.N.R.S., Paris, 24, 138 (1953).

11. Ch'en and Takeo, 1957, Rev. Mod. Phys., 29, 20*.

12. Cooper, J., and Grieg, J.R., Journal of Scientific Instruments, 40, 433 (1963).

13. Dalgarno, A., Intermolecular Forces, Hirschfelder, J.O., ed., John Wiley & Sons, New York, 1967, p. 144.

14. Davis, H.T., Introduction to Nonlinear Differential and Integral Equation, Dover, New York, 1962, p. 209.

15. Day, R.A., Scientific Report No. 18, H.C.O. Shock Tube Laboratory, 1967.

16. Griem, H.A., Plasma Spectroscopy, McGraw Hill, New York, 1964, pp. 98-100.

17. Hindmarsh, W.R., M.N., 119, 11 (1959).

18. Hindmarsh, W.R., Petford, A.D., and Smith, G., Proc. Roy. Soc., A207, 296 (1967).

19. Holtzmark, H., Am. Physik, 58, 577 (1919).

20. Jablonski, A., Phys. Rev., 68, 78 (1945).

21. Klein, L. and Margenau, H., 1959, J. Chem. Phys., 30, 1556.

22. Kusch, H.J, Zs. f. Astrophys., 45, 1 (1958).

23. Lalos, G.T., and Hammond, G.L., Ap. J., 135, 616 (1962).

24. Lindholm, E., Ark. Mat. Astron. Fys., 28B, 3 (1941).

25. Margenau, H., Phys. Rev., 48, 755 (1935).

26. Margenau, H., Phys. Rev., 82, 156 (1951).

27. Margenau, H. and Kestner, N.R., Theory of Intermolecular Force, Pergammon Press, Oxford, 1969.

28. Michele et al, 1959, Physics, 25, 1321.

29. Muller, E., "Composition of the Solar Atmosphere", Solar Physics, Xanthakis, ed., Interscience, 1967, pp. 36 and 40.

30. Parkinson, W.H., and Reeves, E.M., Scientific Report No. 1, H.C.O. Shock Tube Laboratory, 1964.

31. Roueff, E., and Van Regemorter, H., Astron. & Astrophys., 1, 69, (1969).

32. Traving, G., Mit. Astron., Ges., Sonderheft Nr. 1 (1959).

33. Van Regemorter, H., Ann. Rev. Astron. & Astrophys., 3, 90 (1965).

34. Weisskopf, V., Z. Physik, 75, 287 (1932).

FIGURE CAPTIONS

Fig. 1 Schematic representation of the piston compressor and associated measurement apparatus

Fig. 2 Schematic layout of the interferometric technique used to measure N_{He} and N_e

Fig. 3 Calculated compressed gas conditions in Helium for 50 psi driver pressure and 300°K initial temperature in existing tube *

Fig. 4 Calculated compressed gas conditions in Helium for 125 psi driver pressure and 300°K initial temperature in existing tube.

Fig. 5 Calculated compressed gas conditions in Hydrogen for 50 psi driver pressure and 400°K initial temperature in existing tube

Fig. 6 Calculated compressed gas conditions in Hydrogen for 125 psi driver pressure and 400°K initial temperature in existing tube

Fig. 7 Calculated compressed gas conditions in Hydrogen for 50 psi driver pressure, 400°K initial temperature, and only 20 cm. driver on existing tube

Fig. 8 Calculated compressed gas conditions in Hydrogen for 125 psi driver pressure, 400°K initial temperature, and only 20 cm. driver on existing tube

Fig. 9 A. Experimental full half widths of Naλ-5889 in He and suggested extrapolation to lower densities
B. Predicted Van der Waals full half widths of Naλ-5889 in He

* The "existing tube" referred to is the original (~1m driver, 3 m. test section) compressor in which these Naλ-5889 widths were measured. Subsequently a specially designed ~ 8 m. compressor has been constructed for continued experiments in H.

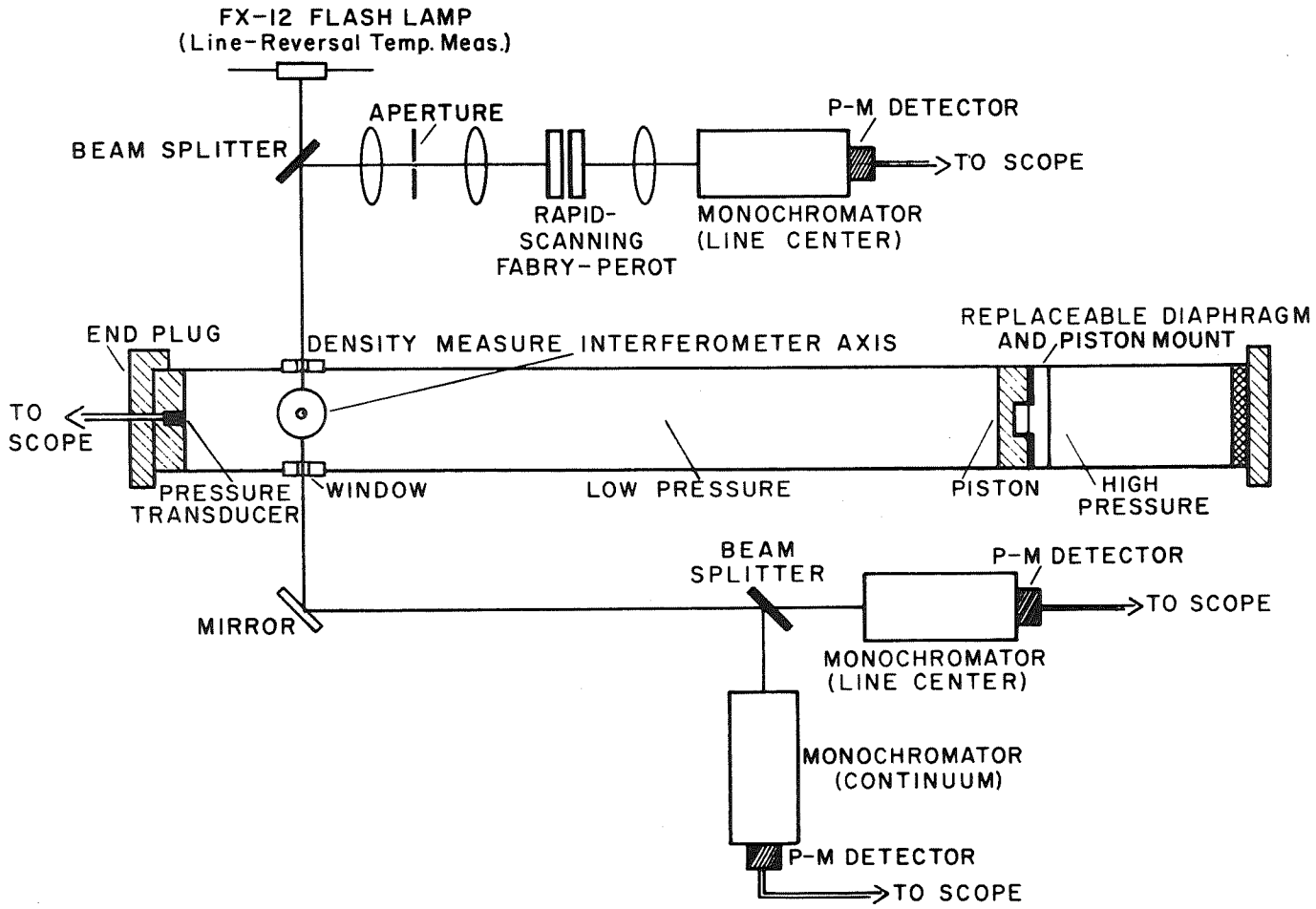

Fig. 1 PISTON COMPRESSOR AND ASSOCIATED MEASUREMENT APPARATUS

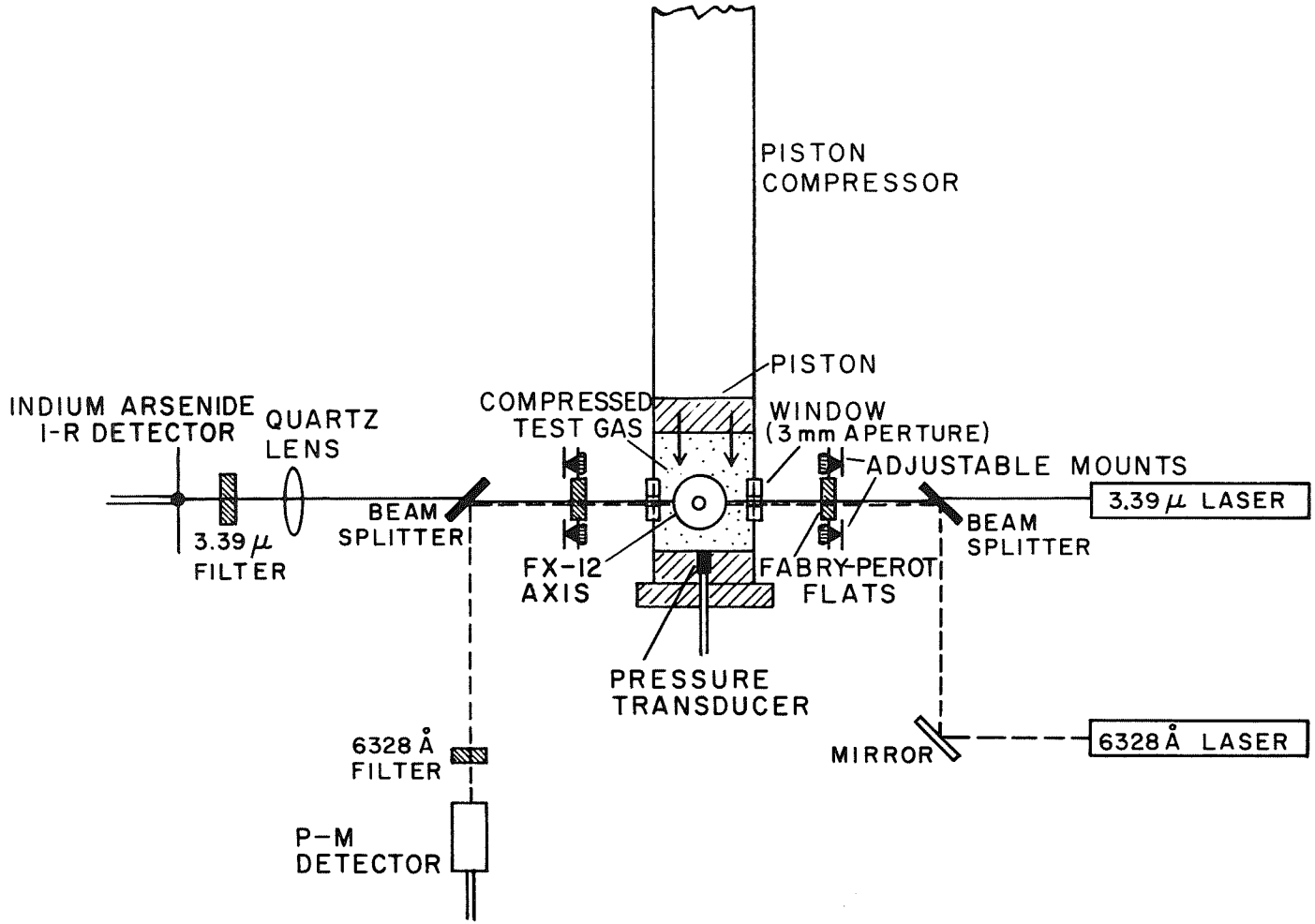

Fig. 2 FABRY-PEROT INTERFEROMETER FOR MEASURING NEUTRAL DENSITIES (6328 Å) AND ELECTRON DENSITIES (3.39 μ)

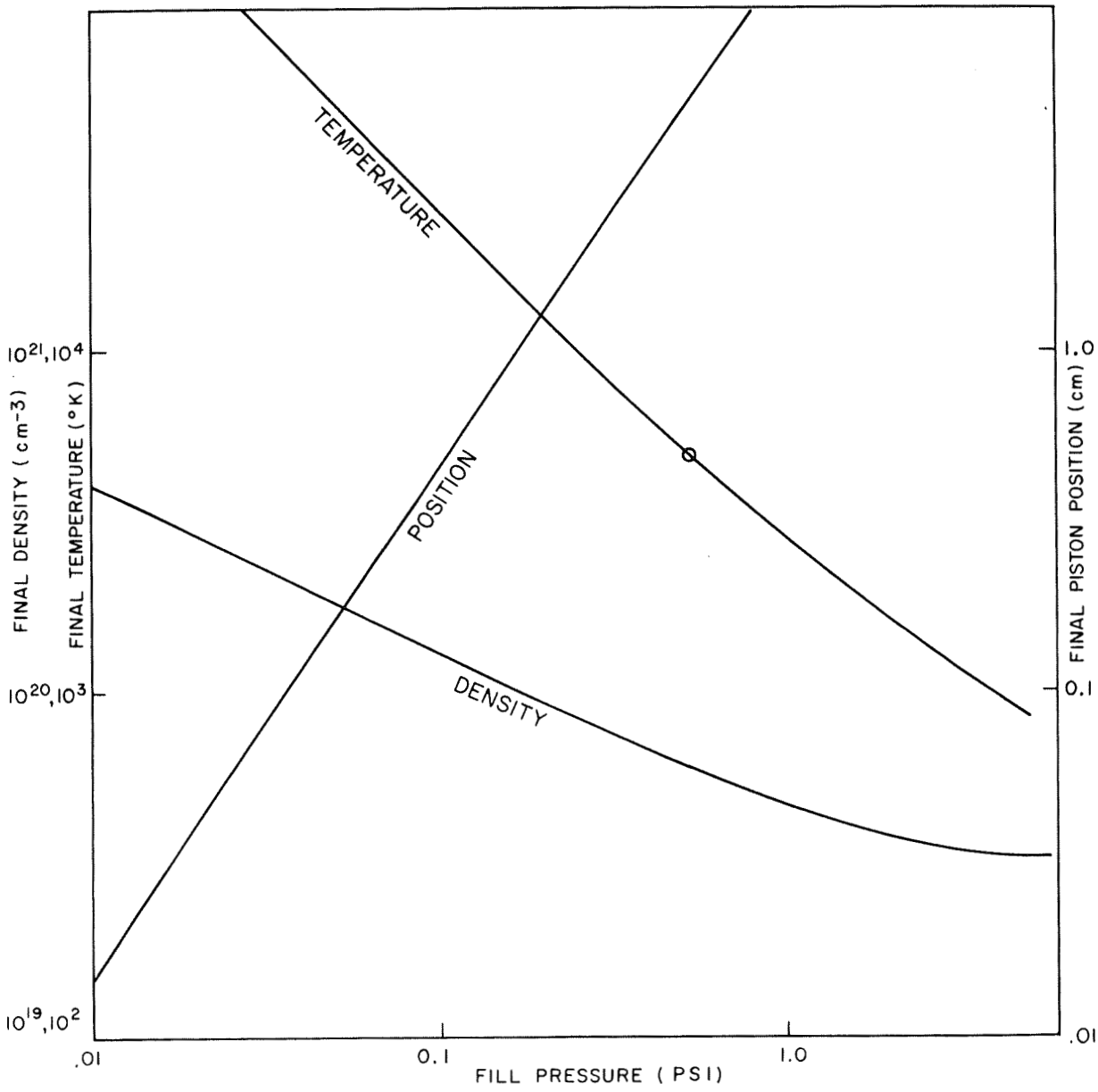

Fig. 3 – HELIUM, P_{DRIVE} = 50 PSI

EXISTING TUBE

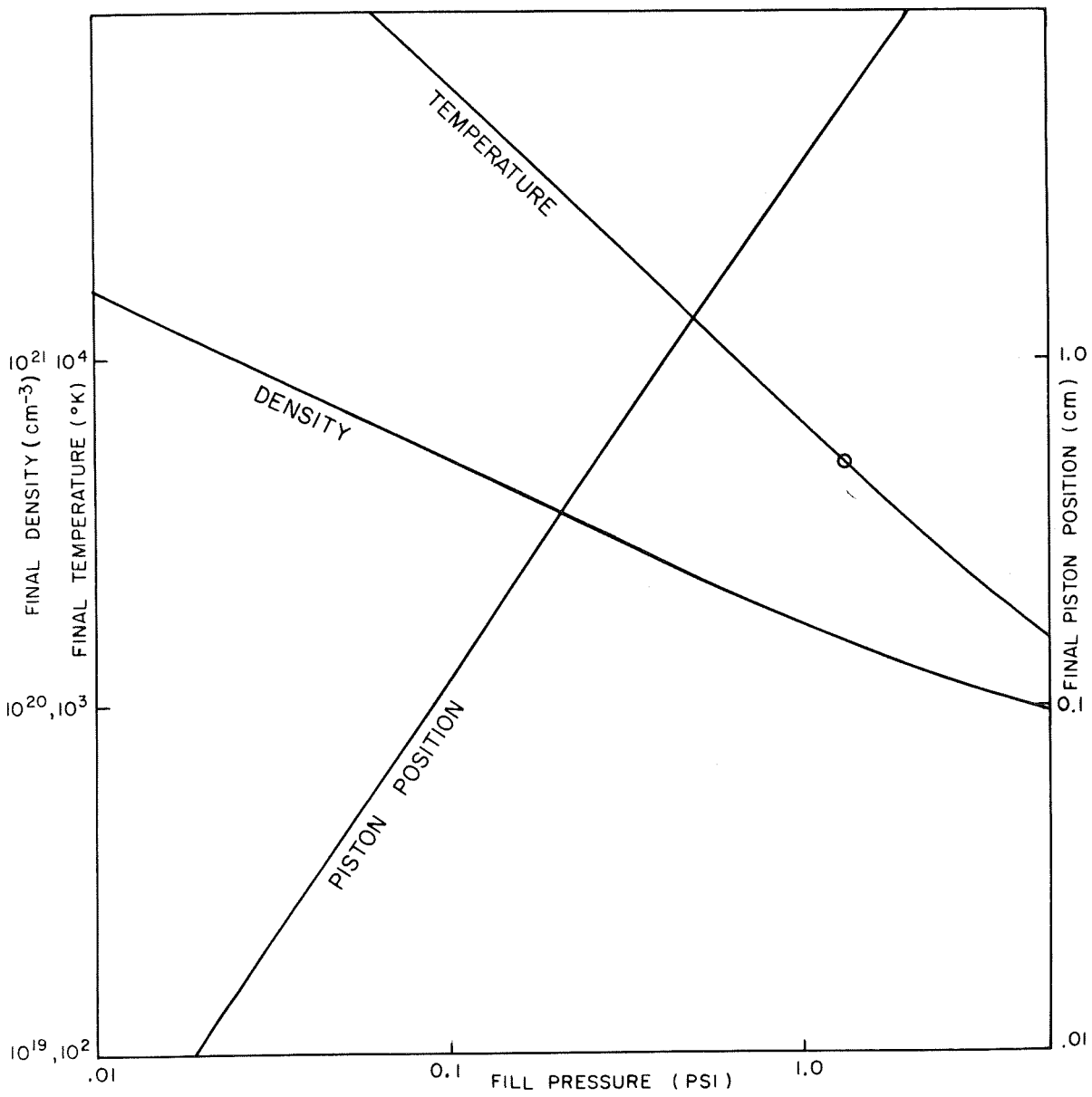

Fig.4 - HELIUM, P_{DRIVE} = 125 PSI

EXISTING TUBE

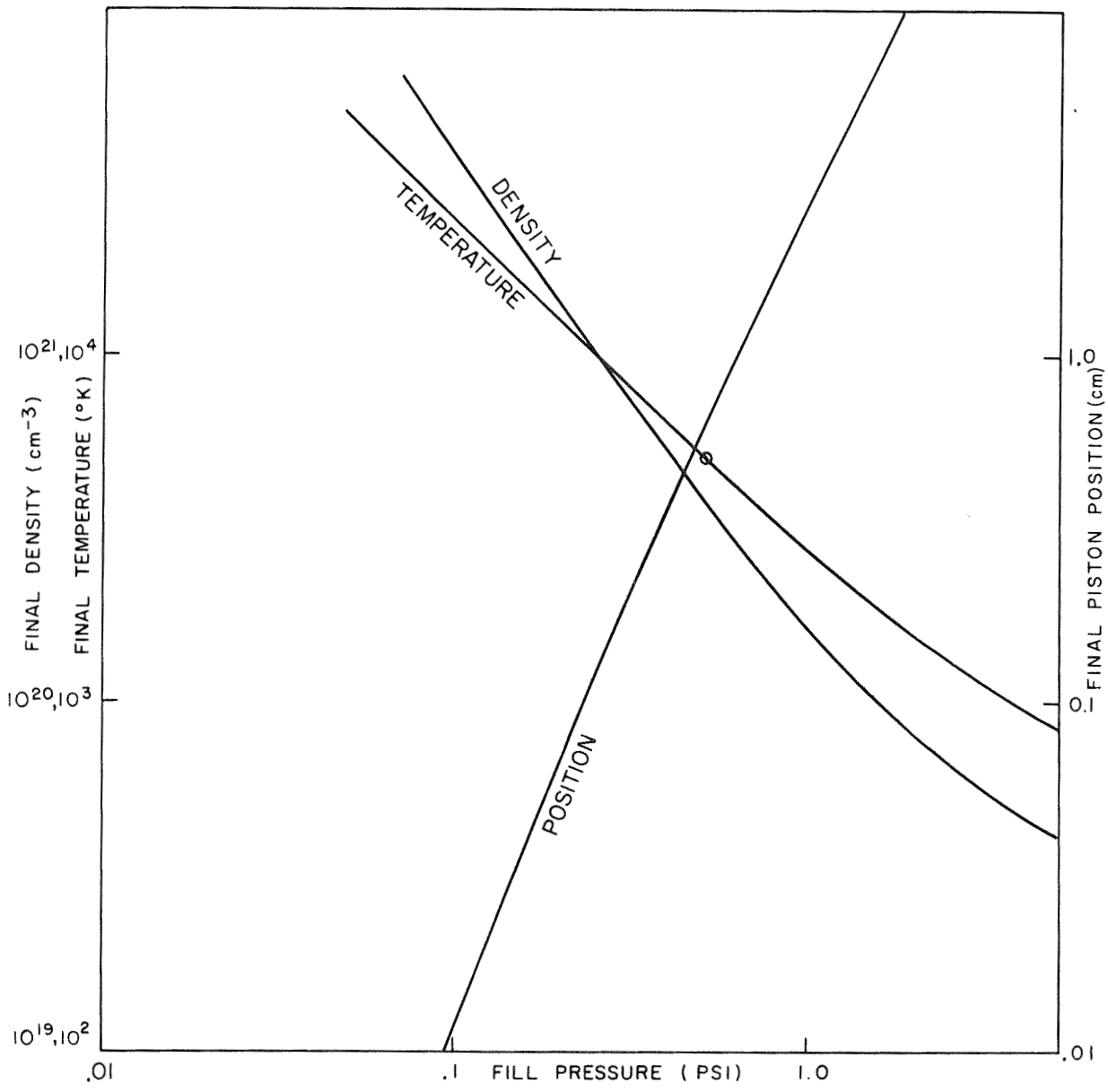

Fig. 5 – HYDROGEN, P_{DRIVE} = 50 PSI

EXISTING TUBE

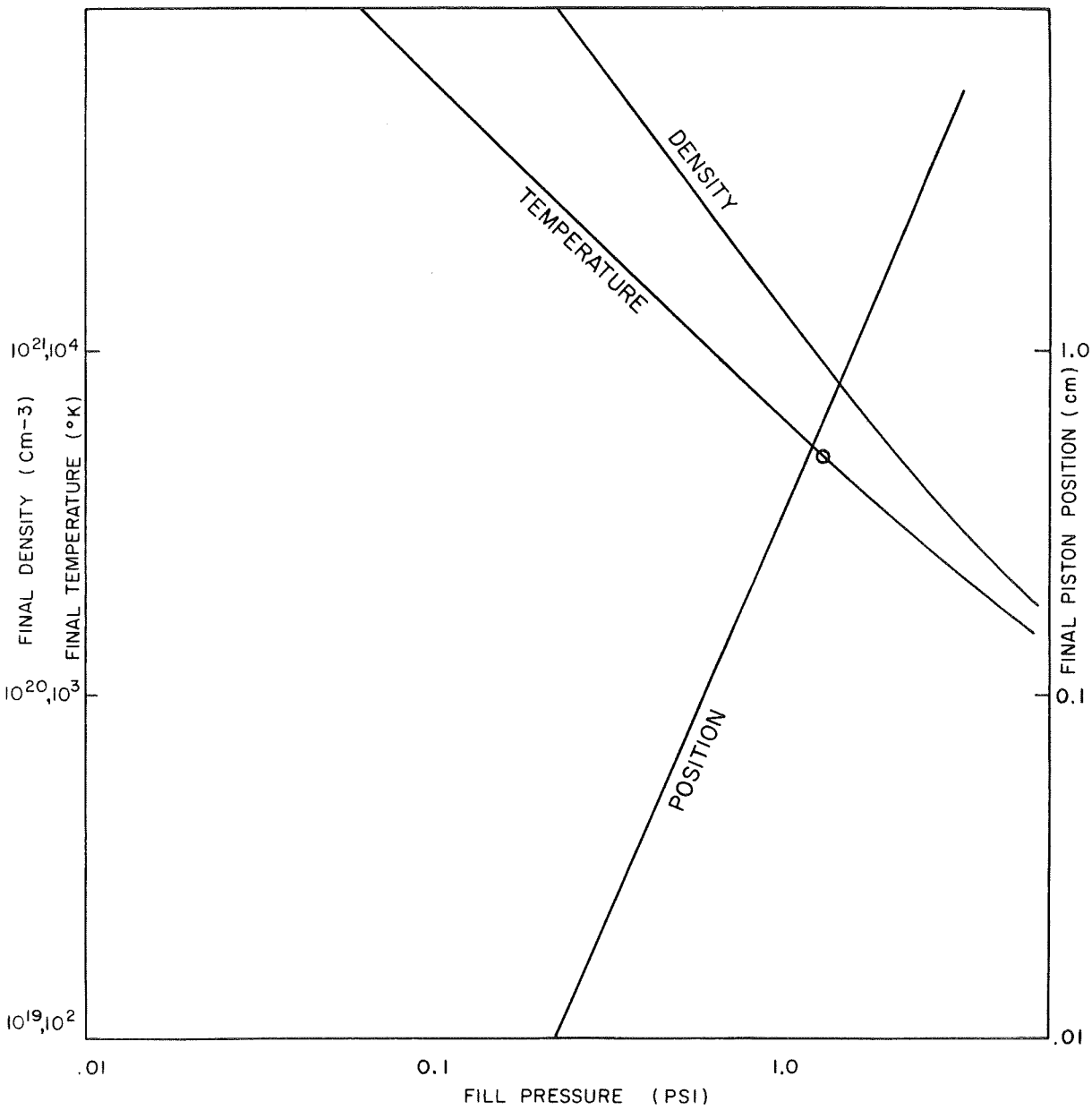

Fig. 6 – HYDROGEN, P_{DRIVE} = 125 PSI
EXISTING TUBE

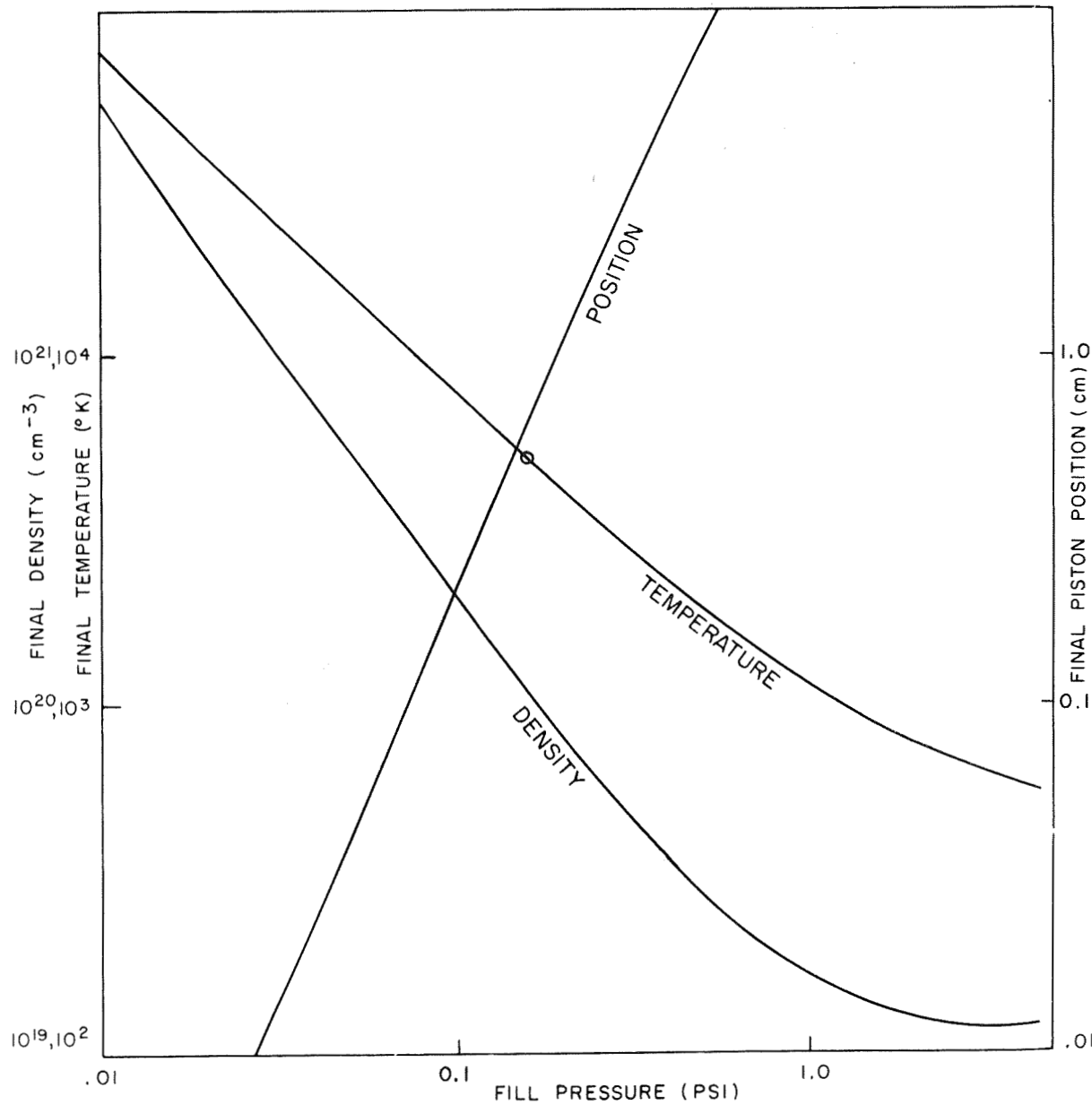

Fig.7- HYDROGEN, P_{DRIVE} = 50 PSI

20 cm DRIVER

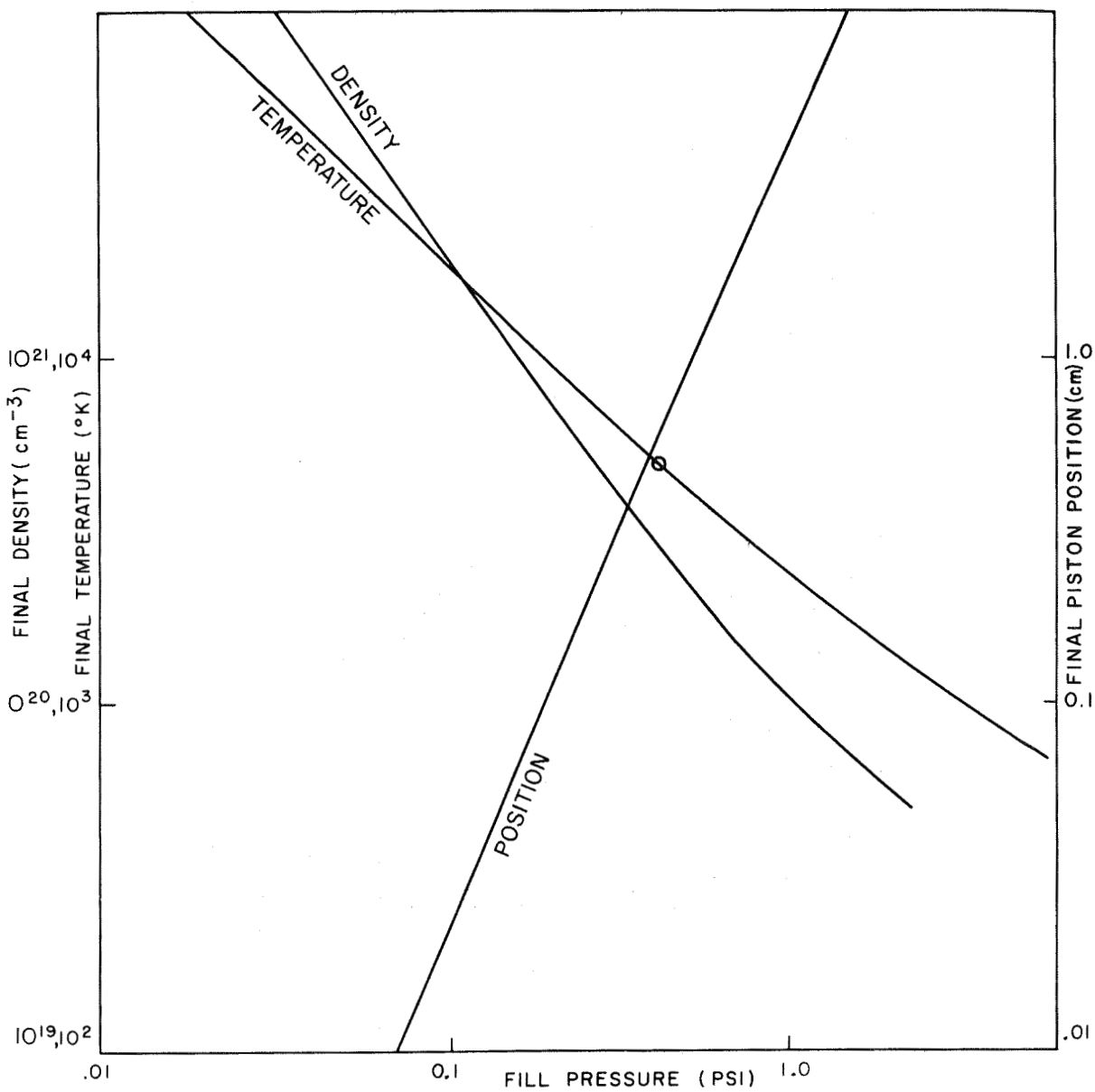

Fig.8-HYDROGEN , P_{DRIVE} = 125 PSI

20 cm DRIVER

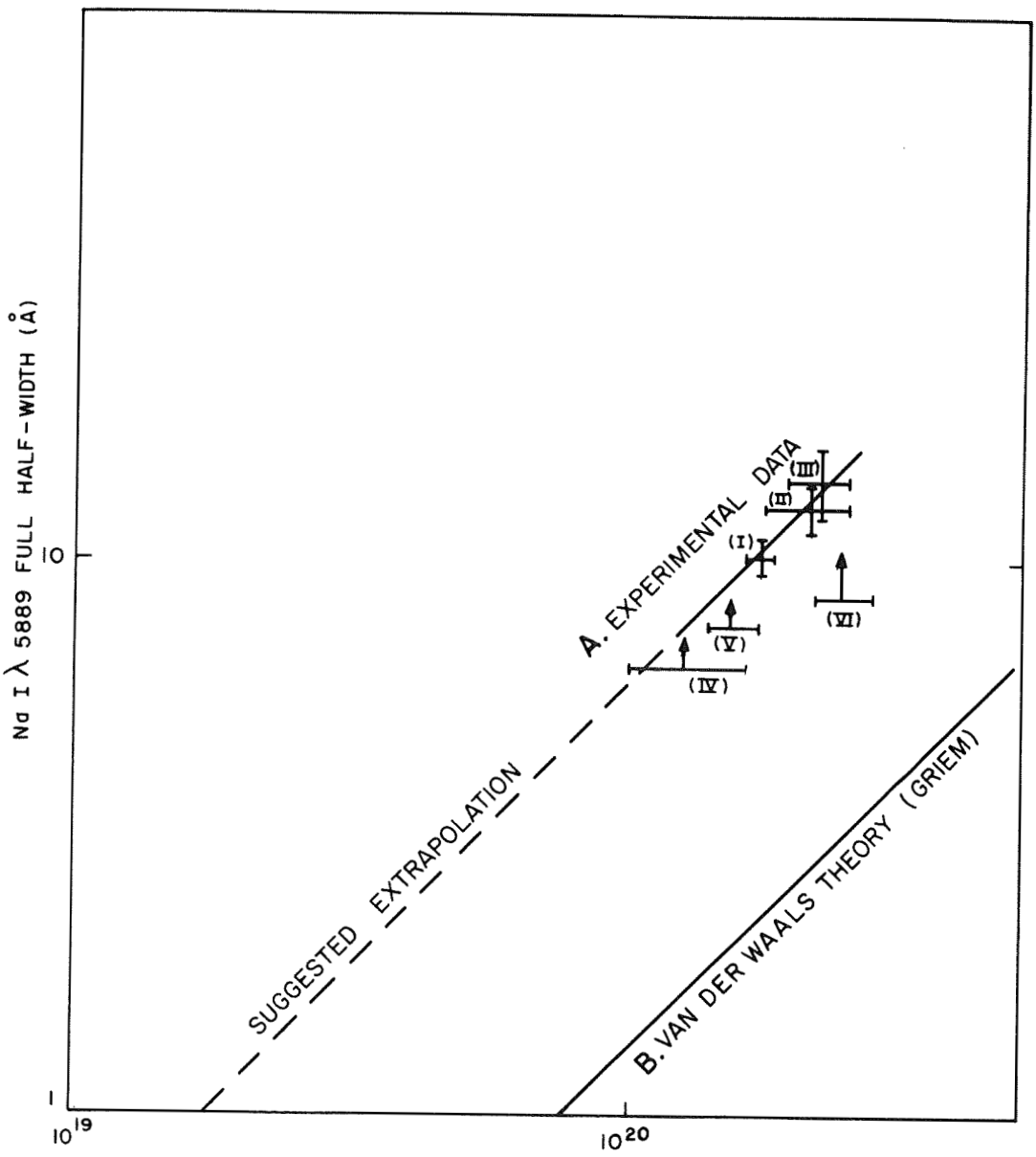

Fig.9 (A&B) HELIUM DENSITY (cm^{-3})